



Global IWV trends and variability in atmospheric reanalyses and GPS observations

Ana C. Parracho^{1,2}, Olivier Bock¹, Sophie Bastin²

¹IGN LAREG, Université Paris Diderot, Sorbonne Paris Cité, Paris, 75013, France,

5 ²LATMOS/IPSL, UVSQ, Université Paris-Saclay, Sorbonne Universités, UPMC, Univ., Paris 06, CNRS, Guyancourt, France

Correspondence to: Ana C. Parracho (ana.parracho@etu.upmc.fr)

Abstract. Water vapour plays a key role in the climate system. However, its short residence time in the atmosphere and its high variability in space and time make it challenging when it comes to study trends and variability. There are several sources of water vapour data. In this work we use Integrated Water Vapour (IWV) estimated from GPS observations and atmospheric reanalyses. Monthly and seasonal means, interannual variability, and linear trends are analysed and compared for the period between 1995 and 2010. A general good agreement is found but this study highlights issues in both GPS and reanalysis data sets. In GPS, gaps and inhomogeneities in the time series are evidenced, which affect mainly variability and trend estimation. In ERA-Interim, too strong trends in certain regions (e.g. drying over northern Africa and Australia, and moistening over northern South America) were found. Representativeness differences in coastal areas and regions of complex topography (mountain ranges, islands) are also evidenced as limitations to the intercomparison of the point observations and reanalysis data. A general good agreement is found for the means and variabilities, with the exception of a few stations where representativeness issues are suspected. Monthly IWV trends are also found to be in good sign agreement, with the exception of a handful of stations where, in addition to representativeness errors, there might be inhomogeneities in the GPS time series. Seasonal trends are found to be different and more intense than monthly trends, which emphasizes the influence of atmospheric circulation on IWV trends. In order to assess strong trends over regions lacking GPS stations, a second reanalysis, MERRA-2, is introduced. The period of analysis is extended to 1980-2016 (the longest period the reanalyses have in common) and differences with the shorter period are found. This exemplifies how much IWV trends are dependent on the time period at study and must be interpreted carefully. Temperature trends are also computed for both reanalyses. The Clausius-Clapeyron scaling ratio is found to not be a good humidity proxy at seasonal and regional scales. Regions over northern Africa and Australia, where ERA-Interim and MERRA-2 disagree, are investigated further. Dynamics at these regions is assessed by analyzing the wind fields at 925 hPa and is shown to be tightly linked with the trends and variability in IWV.

1 Introduction

Water vapour is a key component of the Earth's atmosphere and plays key role in the planet's energy balance. It is the major greenhouse gas in the atmosphere and accounts for about 75% of the total greenhouse effect (Kondratiev, 1972). This is a global



average, as the greenhouse effect of water vapour depends on the total amount of water vapour in the column which is spatially heterogeneous. At global scale, the total amount of water vapour is mainly controlled by temperature following closely the Clausius-Clapeyron (C-C) equation (Held and Soden, 2006; Semenov and Bengtsson, 2002). According to C-C, a temperature increase in the lower troposphere of 1°C leads to an increase in the vertical profile of water vapour of 6 to 7% (globally). It is thus an important part of the response of the climate system to external forcing, constituting a positive feedback in global warming (IPCC report). However, at regional scale, deviations from C-C law are observed and the strength of the feedback can vary, also because the radiative effect of absorption by water vapour is sensitive to the fractional change in water vapour, not to the absolute change.

Integrated water vapour (IWV) has also been shown to be an important parameter in precipitation onset. Neelin et al. (2009), Holloway and Neelin (2009) and Sahany et al. (2012) concluded that IWV is a better proxy than surface humidity, sea surface temperature or integrated column saturation for transition to deep convection in the Tropics because at higher temperatures, deep convection occurs at lower relative humidity rates. Entrainment processes actually play a substantial role in the onset of deep convection, which is thus sensitive to the lower tropospheric humidity. However, the relationship between IWV and precipitation is a two-way interaction since convection also moistens the free troposphere (the upper-troposphere mainly). This relationship is a key issue for models in a warming climate. Bastin et al. (submitted) used it to evaluate simulations performed in the framework of MED-CORDEX (Ruti et al. 2015) over the Mediterranean area and concluded that models with “too light, too often” precipitation could be better constrained by IWV-temperature relationship. Therefore, seasonal, interannual and temperature-IWV variability should be studied.

At these (seasonal and interannual) scales, climate variations also result from natural variability. The spatial structure of climate variability at seasonal and longer time scales evidences patterns that result from interactions between the atmospheric circulation and the land and ocean surfaces. These include the El Niño Southern Oscillation (ENSO) and the North Atlantic Oscillation (NAO). ENSO is a quasi-periodical oscillation in winds and sea surface temperature over the tropical eastern Pacific Ocean, which impacts the weather and climate worldwide. The NAO fluctuates at time scales that go from days to decades, and has an impact over the regional climate variability in Europe, particularly in winter.

Although El Niño events are associated with increasing temperatures in the eastern and central Pacific with impact on the global weather and climate, it is not well known if global warming will lead to more frequent or intense El Niño events (Colins et al., 2010). Conversely, although a high positive NAO (when the gradient between the Icelandic Low and the Azores High is enhanced) is associated with warmer winters in the Eurasian landmass, due to the stronger westerly and south-westerly airflow that brings in warmer maritime air, it is not clear how the phase or intensity of NAO has been, or will be, affected by climate change (Visbeck et al., 2001).

All these parameters, and the fact that the time of residence of water vapour in the atmosphere is short, make IWV a highly variable component and its study in terms of variability and trends are rather challenging. Several studies have reported on the long-term trends obtained from different IWV datasets. Although there appears to be a global positive trend in the overall IWV



data, which is consistent with a global warming trend, it is difficult to compare results from different studies, as they refer to different data sources, time periods and different sites and spatial coverage.

There are several sources of IWV data, including different types of measurements (using instruments such as radiosondes, Global Positioning System (GPS), and satellites), atmospheric reanalyses, and climate models. For studies at the scale of
5 climate change (seasonal, annual and interannual scales), the data must be available long-term, must be consistent and preferably homogeneous over time so as to not include (or reduce) non-climatic influences such as drifts and abrupt changes. Indeed, differences in trend estimates exist between the existing IWV products, due to a lack of homogenized datasets (Ning et al., 2016; Schröder et al., 2016; Wang et al. 2016).

In this paper, GPS-derived IWV data is used. GPS has the advantage of having a growing global network of mostly land-based
10 stations (see Fig. 1), which gather data under most weather conditions, at a high temporal resolution, and with a continuous temporal coverage that dates back to 1995. The GPS data has been consistently reprocessed to ensure a homogeneous retrieval of IWV. However, it can still be affected by inhomogeneities, due to (for instance) changes in GPS equipment and algorithm details (Vey et al., 2009; Ning et al., 2016).

This data is compared with and complemented by data from the European Centre for Medium-Range Weather Forecasts
15 (ECMWF) reanalysis, ERA-Interim, which provides a multivariate, spatially complete, and coherent record of the global atmospheric circulation (Dee et al., 2011), thus a priori a good complement of the more sparse GPS dataset. ERA-interim has been chosen because it is quite recent, is used to drive/force a lot of regional climate simulations, and is often used to assess climate models, which have difficulty in accurately representing the water vapour distribution in the atmosphere, and in describing its greenhouse effect, especially at the regional level.

Nevertheless, with regards to IWV in particular, the homogeneity of the reanalysis data has also been called into question by
20 several studies (Bengtsson et al., 2004; Dessler and Davis, 2010; Schröder et al., 2016). Schröder et al. (2016) compared the IWV from three reanalyses (ERA-Interim; the Modern-Era Retrospective analysis for Research and Applications, MERRA; and the Climate Forecast System Reanalysis, CFSR) with three satellite-based IWV data records (Hamburg Ocean Atmosphere Parameters and Fluxes from Satellite Data, HOAPS; Remote Sensing Systems, REMSS; NASA Water Vapour Project
25 MEaSUREs program, NVAP-M), for the 1988-2008 period. They analysed anomaly differences relative to HOAPS for averages over the global ice-free oceans and found break-points, which mostly coincided with changes in the observing system. In addition, their trend estimates show poor consensus in the central Africa, the Sahara, and South America regions.

The main objective of our paper is thus the inter-comparison and inter-assessment of the global reprocessed GPS IWV data
30 set and ERA-Interim reanalysis with special focus on trends and interannual variability. Trenberth et al. (2005) analysed trends and variability of IWV over the period 1988-2001 and used radiosonde data from Ross and Elliott (1996, 2001) over land to evaluate the ECMWF reanalysis ERA-40 and National Centers for Environmental Prediction (NCEP) reanalyses. However, radiosondes were shown to be in less agreement with ERA-Interim than GPS and DORIS IWV (Bock et al., 2014). In this study, to add new insights in both the evaluation of ERA-interim reanalysis and in the understanding of IWV trends and variability, we separate the analysis into seasons, and consider trends and interannual variability of seasons. This helps to better



identify regions with higher uncertainty and to understand the physical processes involved in different seasons (e.g. dynamical component strongly differ between seasons). A second reanalysis (MERRA-2, Gelaro et al., 2017) is used in complement to ERA-Interim when necessary to shed some light on the processes that are instrumental in explaining errors. Inspection of results from MERRA-2 also helps to assess strong ERA-Interim trends in regions where no GPS data are available (e.g. northern Africa), or where GPS and ERA-Interim are not in agreement.

This paper is organized as follows: the next section details the datasets and methods used. Section 3 reports on the means and variability found in the GPS and ERA-Interim data, for the 1995-2010 period. Section 4 focuses on the monthly and seasonal trends in GPS and ERA-Interim for 1995-2010. In section 5 we confront results of ERA-Interim and GPS to MERRA-2. In this section, the comparison between ERA-Interim and MERRA-2 was also extended to the 1980-2016 period and focused on two regions of intense trends: western Australia and north Africa/eastern Sahel. Section 6 concludes the paper.

2 Datasets and methods

2.1 Reanalysis data

Reanalysis data from the ECMWF, ERA-Interim (Dee et al., 2011), and NASA, MERRA-2 (Gelaro et al., 2017), were extracted for the 1980-2016 period, at their highest horizontal resolution ($0.75^\circ \times 0.75^\circ$ for ERA-Interim and 0.625° longitude $\times 0.5^\circ$ latitude for MERRA-2). In this work, the two-dimensional (2D) distribution of IWV is investigated with reanalysis fields and with point observations from 104 GPS stations of the International GNSS (Global Navigation Satellite System) Service (IGS) network (Fig. 1). Because GPS heights and model surface heights are not perfectly matched (see the GPS coordinates and ERA-Interim heights in the supplement Table S1), the IWV estimates were adjusted for the height difference using two different methods. In the 2D maps (e.g. Fig. 2), the monthly mean GPS IWV estimates were height corrected to match the nearest ERA-Interim grid point, while for the computation of IWV differences (e.g. Fig. 3), a more elaborate interpolation method was used (described below). For the monthly mean IWV correction, specific humidity from the ERA-Interim pressure level data was integrated over the layer of atmosphere bounded by the model's surface height and the height of the GPS station. The ERA-Interim pressure level data contains a total of 37 levels between 1000 and 1 hPa, and 27 levels between 1000 and 100 hPa. This ensures a good vertical sampling of the troposphere where most of the water vapour is located. The height differences between GPS stations and nearest model grid points range from -1457 m (at the SANT (Santiago, Chile) station) to +3167 m (at the MKEA (Mauna Kea, Hawaii) station). The negative height difference means GPS height is below the model surface. The mean IWV corrections for these two stations amount to -3.4 kg.m^{-2} and 21.7 kg.m^{-2} , respectively. Globally, 102 out of the 104 stations have a correction smaller than 7.7 kg.m^{-2} in absolute value and the inter-quartile range is $[-1.40, 0.39] \text{ kg.m}^{-2}$.

A more rigorous approach is adopted for the quantitative evaluation of the reanalysis IWV data with respect to GPS IWV data, in order to minimize temporal and spatial sampling issues. In this case, we time-matched the 6-hourly data and performed a spatial interpolation of the reanalysis IWV estimates to the latitude and longitude of the GPS site. A bilinear spatial



interpolation is computed from the model IWV estimates at the 4 grid points surrounding each GPS station. The IWV model estimates are then recomputed from the pressure level data by vertically integrating the specific humidity between the height of the GPS station and the top of the atmosphere. Most GPS station heights fall between two pressure levels and the specific humidity data can be interpolated. However, for stations located below 1000 hPa (the lowest pressure level) the reanalysis data are extrapolated. Interpolation and extrapolation are done linearly for specific humidity and temperature, and exponentially for pressure. This procedure minimizes differences between the reanalysis IWV data and the GPS estimates with better results than previous correction methods (e.g. Bock et al., 2014). However, a perfect match between observations and model data is hindered by representativeness errors (Lorenz, 1986), especially in mountainous and coastal regions.

2.2 GPS data

The reprocessed GPS data set used in this work was produced by the NASA Jet Propulsion Laboratory (JPL) in 2010-2011. Basic details on the operational GPS data processing procedure are described by Byun and Bar-Server (2009). Compared to the operational version, the reprocessed data set is produced with more recent observation models (e.g. mapping functions, absolute antenna models) and consistently reprocessed satellite orbits and clocks (IGSMail-6298). Inspection of file headers revealed that the processing options were not updated for a small number of stations for a period of nearly one year between March 2008 and March 2009. The comparison of solutions with old and new processing options (available for year 2007) showed that this inconsistency in the processing has negligible impact at most stations, except for stations at high southern latitudes (e.g. in Antarctica). The data set covers the period from January 1995 to December 2010 for 456 stations. Among these, 120 stations have nearly continuous time series over the 15-year period. However, the geographical distribution is quite unequal between hemispheres and even within a given hemisphere., with namely a cluster of 20 stations in the western USA with inter-station distance smaller than 0.75° . In order to avoid over-representation of this region, 16 out of these 20 stations have been discarded (the selection retained those with the longer time series). The final GPS IWV dataset used in this study is thus limited to the selected 104 stations.

The basic observables in this study are the Zenith Tropospheric Delay (ZTD) estimates available at a 5 minute rate. The ZTD data were screened using an adaptation of the methods described by Bock et al. (2014) and Bock et al. (2016). First, we applied a range check on the ZTD and formal error values using fixed thresholds representing the spatial and temporal range of expected values: 1 – 3 m for ZTD and 0 – 6 mm for formal errors. Second, we applied an outlier check based on site-specific thresholds. For ZTD, values outside the median ± 0.5 m are rejected and, for formal errors, values larger than 2.5 times the median are rejected. The median ZTD and formal error values are updated yearly. Using these thresholds, we detected no ZTD values outside the limits. This is because the limits were sufficiently large to accommodate for the natural variability of ZTD values (Bock et al., 2014). On the other hand, the formal error check rejected 8.8×10^{-4} (i.e. less than 0.1%) of the data overall. After screening, the 5-minute GPS ZTD data were averaged in 1-hourly bins.

The conversion of GPS ZTD to IWV was done using the following formula: $IWV = ZWD \times \kappa(T_m)$. Where $\kappa(T_m)$ is a function of weighted mean temperature T_m , and ZWD is the zenith wet delay, obtained from: $ZWD = ZTD - ZHD$ and ZHD is the



hydrostatic zenith delay (see Wang et al. (2005) or Bock et al. (2007) for further details). In this work, the surface pressure used to compute ZHD and the temperature and humidity profiles necessary to obtain T_m were computed using ERA-Interim pressure level data, using a procedure similar and consistent with the IWV integration explained above. The profile variables are first interpolated or extrapolated to the height of the GPS stations at the 4 surrounding grid points and then interpolated bi-linearly to the latitude and longitude of the GPS stations. At this stage, the GPS and ERA-Interim data were time-matched (within ± 1 hour) for both the ZTD to IWV conversion and IWV intercomparison. Based on our experience, this methodology of ZTD data screening and conversion into IWV is the most elaborate and accurate to date.

Afterwards, monthly means of the 6-hourly IWV estimates are computed and those months which have less than 60 values (i.e. at least half of expected monthly values) are rejected. Seasonal means are computed from the monthly values when at least 2 out of 3 months are available. These selection criteria ensure that the computed values are representative of the monthly and seasonal means.

In this work, inhomogeneities in the GPS IWV time series due to equipment changes were not corrected a priori, as the existing metadata is not complete, but were rather detected and discussed during the course of the intercomparison with ERA-Interim. This work is a preliminary contribution to a more extensive detection and correction effort of the GPS IWV data.

2.3 Computation of trends

The linear trends were computed using the Theil-Sen method (Theil, 1950 & Sen, 1968), a non-parametric statistic that computes the median slope of all pairwise combinations of points. This method was found to be more robust than the least square fitting (Rousseeuw and Leroy, 2003), as it is less sensitive to outliers in the time series and does not require a normal distribution of the data. In addition, Wang et al. (2016) found this method to be less sensitive to the start and ending of time series with sparse data (a concern when using the GPS data, with gaps).

The Theil-Sen method was applied to the anomalies obtained by removing the monthly climatology from the monthly data. In the case of seasonal trends, the mean anomalies for the months of December, January and February (DJF); and June, July and August (JJA) were used (when there are at least two months of data available per season). The statistical significance of the monthly and seasonal trends was assessed using a modified Mann-Kendall trend test (Hamed and Rao, 1998), which is suitable for autocorrelated data, at a 10% significance level.

3 Means and variability in GPS and ERA-Interim IWV (1995-2010)

The ERA-Interim and GPS data have been used to investigate the mean seasonal IWV distribution and its interannual variability for December-January-February (DJF) and June-July-August (JJA).

Globally, the mean IWV (Figs. 2a, b) is strongest in the tropics where strong evaporation occurs from the warm oceans and land surface and where trade winds transport moisture to the Intertropical Convergence Zone (ITCZ). Lower evaporation occurs at mid and high latitudes due to the cooler oceans and land surface. Lower IWV observed at these latitudes is also explained by the limited moisture-holding capacity of the relatively cooler tropospheric air (Trenberth et al., 2007; Lorentz



and DeWeaver, 2007). The rapid decrease of water vapour saturation pressure with altitude as predicted by Clausius–Clapeyron equation also explains the lower IWV contents over elevated land surfaces. Minimal IWV values are found over major mountain ranges (e.g. the Himalayas and the Andes cordillera). The lack of surface water is another strong limitation for evaporation and thus atmospheric humidity as observed in arid regions (e.g. Sahara, Arabic peninsula, south-eastern Africa, Australia). Strong seasonal variation is driven by the movement of the incoming solar radiation from one hemisphere to the other and back along the course of the year. The resulting global swinging of the trade winds and ITCZ across the Equator is a cause for the regional wet monsoon seasons usually associated with rainfall (e.g. India and southern Asia, West Africa, and southern North America in JJA; northern Australia, central and southern Africa, and the central Amazon River basin in South America in DJF). The high rainfall patterns (not shown) coincide well with the high IWV patterns shown in Fig. 2.

For the analysis of the interannual variability we computed the relative standard deviation of the seasonal IWV time series (i.e. standard deviation of seasonal time series divided by its mean value). The relative variability emphasizes both regions where the variability is high compared to the mean IWV (e.g. the tropics) and regions where the mean IWV contents are small (e.g. cold dry polar and/or mountainous regions and warm dry desert areas). In DJF (Fig. 2c), strong interannual variability ($> 15\%$) is found for northern high-latitude regions (north-eastern Canada and eastern Greenland, polar Arctic area, and a large part of Russia and north-eastern Asia) and for the tropical arid regions (Sahara, Arabic peninsula, central Australia). Some correlation is found between the seasonal IWV anomalies and the North Atlantic Oscillation (NAO) index (Barnston and Livezey, 1987) are found (not shown) over Siberia ($r = 0.5$) and Greenland ($r = -0.5$). Noticeable variability is also seen in the central tropical Pacific in DJF but this is due to the extremely large variability in absolute IWV contents (up to 6 kg.m^{-2}) associated with the ENSO. Linear correlation coefficients between the seasonal IWV anomalies and the Multivariate ENSO Index (MEI; Wolter and Timlin, 1993, 1998) in this region reach $r = 0.80$ (not shown). In JJA, large interannual variability is observed mainly over Antarctica and Australia (Fig. 2d). Locally enhanced variability is also seen over the Andes cordillera, but this is mainly due to the very low IWV values at high altitudes.

In general, there is good agreement between ERA-Interim and GPS. In the maps of the means (Figs. 2a, b), we can see that ERA-Interim reproduces the spatial variability well, including the sharper gradients in IWV, for instance, on the northern and southern flanks of the ITCZ in both seasons, and in the regions of steep orography (for example, along the Andes region, in South America).

The mean IWV differences are shown in Figs. 3a and b for all 104 GPS sites. It can be noticed that negative differences (ERA-Interim drier than GPS) are almost all located approximately within the ITCZ, with few exceptions in north-western North America and in Antarctica. A paired two-sample t-test detected 20 stations with significant differences in the mean IWV values at 0.01 confidence level in DJF and 17 in JJA (the values for all stations can be found in Supplement Table S2). The sites with most notable differences, either absolute (in kg.m^{-2}) or relative (in %) are: CFAG in the Andes cordillera with a bias of 6.5 kg.m^{-2} (26%) in DJF and 3.9 kg.m^{-2} (43%) in JJA and, SANT in Chile with -2.4 kg.m^{-2} (-15%) in DJF, and TSKB (in Japan) with 1.9 kg.m^{-2} (24%) in DJF. In JJA, four other sites have large biases: KIT3 in Uzbekistan with a value of 6.2 kg.m^{-2} (35%), POL2 in Kirghizstan with 3.1 kg.m^{-2} (20%), SYOG in Antarctica with 0.6 kg.m^{-2} (32%), and MAW1 in Antarctica with 0.4



kg.m⁻² (31%). Results for all the stations can be found in Table S2 of the Supplement. The inspection of the time series shows that at some of these stations the biases are not constant in time but contain large seasonal variations, such as e.g. at CFAG (Fig. 4a) or KIT3 (Fig. 4b). These sites are located in coastal regions and/or regions with complex topography. Although we used an elaborate spatial and temporal matching of reanalysis and GPS data, representativeness errors are suspected to be the cause of these biases. To investigate this point, we compared the (vertically adjusted) IWV values from the 4 grid points surrounding each GPS station to the interpolated IWV values (see section 2). We found that at CFAG, KIT3, POL2, SYOG, and MAW1, the interpolated values did not minimize the IWV biases between the reanalysis and GPS. This is explained by large variations in the altitude of the grid points at these sites (between 500m and 1000m) and the difficulty for the vertical interpolation method to properly predict the IWV variations over such large altitude ranges. In the case of SANT, although the interpolated value matches the GPS value better than any of the four surrounding grid point values, there is still a large bias explained by a variation in the altitude of the grid points of over 1500m. Statistics computed over all stations are given in Table 1. They indicate that ERA-Interim is slightly moister on average than GPS. The median bias is 0.51 kg m⁻² (6.2%) in DJF and 0.52 kg.m⁻² (2.7%) in JJA, and the standard deviation of the bias across the network amounts to 0.83 kg.m⁻² (6.9%) in DJF and 0.95 kg.m⁻² (7.8%) in JJA. As noticed above, there is some spatial variation in the mean difference, namely a negative mean difference in the tropics (ERA-Interim < GPS) which is compensated in the global median by the larger number of stations in the extra-tropics which have a positive difference (ERA-Interim > GPS).

Most of the marked regional features of interannual variability are also confirmed by GPS observations (Figs. 2c, d). One can especially notice the good representation of the relative variability over Australia or South America, both in DJF and JJA, and in the northern high latitudes, where the gradients are strong and well captured. However, a few stations show different values compared to the ERA-Interim background. Figures 3c and d show the differences of relative standard deviations. The overall statistics are given in the second part of Table 1. They indicate a median difference close to zero for both DJF and JJA with a standard deviation across the stations of 1.7% in DJF and 4.1% in JJA. We used a two-sample F-test to detect the stations where the variances differ significantly. However, this test detected only one result with a p-value < 0.01 (station MCM4 in JJA) and two with a p-value < 0.10 (MCM4 and CFAG in JJA). This statistical test is probably not very efficient in the case of our short time series (≤16 points). In JJA, the four stations with the largest differences (ERAI – GPS) are located in Antarctica: MCM4, SYOG, MAW1, and DAV1 with differences of -39% (p=0), -7.7% (p=0.63), -4.8% (p=0.81), and +3.9% (p=0.27), respectively. In DJF, the largest differences are found for MKEA (Hawaii) and SYOG, where they amount to -11.4% (p=0.52) and -4.8% (p=0.30), respectively. Table S2 in the supplement provides the results for all stations. In the case of SYOG, MAW1, and DAV1, representativeness errors are suspected again because of the large variability in the IWV values of the surrounding grid points connected with large variations in the altitudes (> 500m) of these grid points. In the case of MKEA, the variation in the altitude of the surrounding grid points is quite small because of the limited imprint of Mauna Kea Island on the 0.75° resolution grid of ERA-Interim. However, the difference in altitude between the GPS station and all four grid points is larger than 3000 m which is far beyond the prediction capability of the interpolation method described in Section 2. In the case of MCM4 and SYOG, the inspection of the time series of monthly mean IWV and IWV differences (shown in



Figs. 4c and d) reveals variations in the means which coincide with GPS equipment changes and processing changes and unexplained variations in the amplitude of the seasonal cycle resulting in a marked oscillation in the monthly mean differences (ERA-Interim – GPS). Variations in the means introduce a spurious component of variability in the GPS IWV series (e.g. at MCM4 the standard deviation of GPS IWV is 0.78 kg m^{-2} compared to 0.21 kg m^{-2} for ERA-Interim).

- 5 Three possible causes for the differences in the IWV means and variability between GPS and ERA-Interim exist. As already discussed above, representativeness differences are expected in regions of complex terrain where the environmental conditions can differ. Strong horizontal gradients in IWV are a limitation for the bi-linear horizontal interpolation that we used. This kind of situation is generally encountered when the altitudes of the grid points surrounding the stations are very different (e.g. AREQ, SANT, KIT3, MAW1, SYOG, POL2). This problem is enhanced when the altitude of the GPS station is below the model surface (e.g. SANT, AREQ, KIT3, MAW1, SYOG), because the model profile data are extrapolated below the ground, and/or the model and GPS surface altitudes are very different (e.g. MKEA). Representativeness errors due to large spatial variations in IWV and altitude are expected at 20 stations among which are those cited just above. However, they don't explain all the significant biases and differences in variability actually observed. The second aspect is connected with errors in the GPS data, e.g. due to instrumental malfunctioning or measurement interferences, or changes in equipment resulting in variations in the mean IWV estimates. Such problems can be detected by comparison with IWV measurements from nearby GPS receivers or from other collocated instruments such as DORIS or VLBI (Bock et al., 2014; Ning et al., 2016). The third cause stems from errors in the reanalysis IWV data which are expected in data-sparse regions and regions where the performance of model physics and dynamics are poor. These can be diagnosed by comparing several reanalyses based on different models and different observational data or hypothesized by eliminating the other causes.

20 **4 Trends in GPS and ERA-Interim IWV (1995-2010)**

- Next, taking into account the previous results, the ERA-Interim and GPS data were used to study the trends in IWV over the period 1995-2010. Results from ERA-Interim based on the full monthly time series are discussed first (Fig. 5). Over ocean, generally significant positive trends (moistening) are observed over most of the tropical oceans and over the Arctic. Significant negative (drying) trends are observed in south-tropical eastern Pacific region, west of the United States and generally south of 25 60°S . The dipole structure in the south-eastern tropical Pacific area is consistent with the findings of Mieruch et al (2014) and is due to the different ENSO phases for this time period, as reported by Trenberth et al (2005). Over land, significant positive trends are observed in equatorial region along the ITCZ, especially in northern South America, Central Africa, and Indonesia, and in the northern hemisphere, especially over northern North America, Greenland, most of Europe and Siberia. Significant negative trends over land are observed over North Africa, Australia, Antarctica, central Asia, south of South America, and 30 most of the USA. In general, there is continuity between oceanic and continental trends (e.g. North and South America, Central Africa), suggesting a trend in air mass advections. However, the magnitudes of the larger trends (e.g. -3.5 kg m^{-2} per decade or -17% per decade over northern Africa) are questionable. To be physically explained such trends would imply a significant



change in the regional and global water cycle. Alternatively, they might be due to inhomogeneities in the observations assimilated in the reanalysis system. Comparison to GPS observations, when they are available, helps to address this question. In general, the monthly trends computed at the GPS stations are in good agreement with ERA-Interim (Fig. 5). Many stations are operated in Europe and North America. Most of them show fairly consistent trends with ERA-Interim even in areas of marked gradients (e.g. between western Canada and the USA, or from central to western Europe). Australia is also well documented with several stations, in the centre and along the coasts, and good agreement is found both in the sign and spatial variations of trends. The eastern Australia's moistening trend, although not significant in ERA-Interim, is also observed by GPS. Many isolated stations in other regions confirm the ERA-Interim trends. Moistening trends are observed by stations (indicated in Fig.1) KOUR and BRAZ (northern part of South America), HRAO (South Africa), IISC (India), KELY (Greenland), DGAR (in the centre of the Indian ocean), FALE (in the Pacific ocean), CRO1 (Puerto Rico), MAS1 (Canary Islands) and REYK (Iceland). In terms of drying trends, ERA-Interim and GPS trends are largely in agreement over the west coast of the United States, the southern half of South America (including the Andes region, which has steep IWV gradients) and the western half of Australia. It is also noteworthy that BRMU (in Bermuda) has a drying trend that is also captured in the ERA-Interim data. Overall, GPS absolute trends are greater (in arithmetic sense) than ERA-Interim trends at 62 sites out of 104, while relative trends in GPS are greater than in ERA-Interim at 65 sites out of 104 (see the results for all stations in the supplement Table S3).

Inspection of Fig. 5 shows that there are a number of GPS stations where the trend estimates are large and of opposite sign compared to ERA-Interim: CCJM (south of the Japanese home islands), DARW (northern Australia), WUHN (eastern China), IRKT (central Russia), ANKR (Turkey), KOKB and MKEA (Hawaii), and MCM4 (Antarctica). Some of them (DARW, ANKR, KOKB, MKEA) are located in areas where the ERA-Interim trends change sign and a perfect spatial coincidence between the reanalysis and observations might not be expected. On the other hand, stations CCJM, WUHN, IRKT, and MCM4 are located within regions where the ERA-Interim trends are strong and significant, and extend over large areas. For some of these stations, the discrepancy is due to gaps and/or inhomogeneities in the GPS time series which corrupt the trend estimates. To mitigate the impact of gaps, time-matched series are also compared (Figs. 6a and b show the trend differences). The agreement is improved at DARW, ANKR and IRKT, and at many other sites (e.g. KELY in Greenland, SANT, MAW1). However, there are still many sites with large differences. Table 2 lists the stations with the largest differences. Inspection of time series reveals the presence of large inhomogeneities at CCJM, MCM4 (already discussed in the previous section, see Fig. 4c, WUHN, SHAO, and CRO1. At CCJM (see Fig. 6a), the GPS minus ERA-Interim IWV difference time series has a large offset in 2001 which coincides with a GPS equipment change (receiver and antenna). This offset is responsible for a large negative trend estimate in the GPS series (-1.40 kg m^{-2} per decade) whereas the time-matched ERA-Interim series gives a positive trend ($+0.98 \text{ kg m}^{-2}$ per decade) consistent with the large-scale trend in the reanalysis seen in Fig. 5a. At WUHN (Fig. 7b), the GPS trend estimate is positive (0.34 kg m^{-2} per decade) while the ERA-Interim estimate is negative (-1.45 kg m^{-2} per decade). The IWV difference time series shows several breaks (in 1999, 2005 and at the end of 2006) though none of them coincides with known GPS equipment changes. At this site it is not clear if the inhomogeneity is in the GPS data or in ERA-



Interim. This case will be further discussed below when trends from MERRA-2 reanalysis are analysed (section 5). At SHAO and CRO1, and a few other sites (e.g. SYOG, DARW, ANKR) inhomogeneity in the IWV difference series coincide with documented GPS equipment changes (not shown). Representativeness differences are suspected at mountainous and coastal sites (e.g. AREQ, CFAG, KIT3, MAW1, SANT, SYOG and the other sites discussed in the previous section). Some sites show also more gradual drifts in the times series which don't seem connected with known GPS equipment changes (e.g. MAW1, Antarctica). At such sites, drifts in the reanalysis are plausible and will be further discussed below when MERRA-2 results are analysed.

Wang et al. (2016) studied nearly the same period (1995-2011) by using radiosonde and GPS data over land and microwave (MWR) satellite data over oceans. Over the oceans, results that are significant in ERA-Interim are in good agreement with those obtained by Wang et al. (2016), despite the fact that they are not always significant in the latter study. Over land, none of the values computed by Wang et al (2016) are significant but the drying over western Australia is also observed. No results are obtained over most of Africa and the north-western part of South America due to a lack of data. The drying for north-eastern Africa and moistening over central Africa and north-western South America are therefore not confirmed by the Wang et al. (2016) study. For the other continental areas with weaker trends, results are not always in agreement, for instance over central Asia, where a moistening trend is generally observed in Wang et al. (2016). The western part of USA presents a strong spatial variability in both studies but results are generally not consistent locally. Greenland trends also present opposite signs, even though very low values are obtained in both cases. When comparing with the GPS results obtained by Wang et al. (2016), there is a general good agreement, with some differences in central Australia (ALIC station) and Iceland (REYK). These differences may be due to the extra year in their analysis (as differences in the beginning and ending of time series have an impact on the trend estimation, especially when trends are of low intensity and not significant, and the period at study is relatively short (16 years in our study)).

Although the study does not concern the same period, Trenberth et al (2005) reported similar trend signs to ERA-interim over Africa and South America in the NVAP data (1988-2001) and positive trends over western Pacific, the Indian and Atlantic oceans with SSM/I data (1988-2003). As discussed above, differences are observed over Eastern Pacific where El Niño events strongly affect the trend estimates. Note also a difference in the sign of the trend over Australia (an area which will be discussed later). Wagner et al. (2006) studied the IWV trends in satellite observations from the Global Ozone Monitoring Experiment for the 1996-2002 period. Although their study period is short, they also found positive IWV trends over the western tropical Pacific Ocean and large parts of the southern oceans, and negative trends over North Africa. Over northern Australia, they found a negative trend, which is in agreement with what we obtain but not with Trenberth et al. (2005). This area is thus likely sensitive to the period at stake. The western part of the USA is also an area where differences between the studies are present, but it seems that spatial variability is strong and thus results strongly depend on the resolution of the datasets, and not only on the period. Thus, despite the different periods and the use of different observing systems, some areas show consistent trend



signs with ERA-Interim which indicates that the results are likely robust. However, the trends obtained in our study can differ from those presented by other authors for other periods, as the trend estimation is highly dependent on the time period at study. To better understand the trends, we separated them by seasons (DJF or JJA), which are presented in Figs. 8a and b, respectively. A striking feature of the seasonal trends is their relatively larger magnitude compared to the monthly trends. Large changes in magnitude and/or sign are also noticeable in most regions. These features emphasize that atmospheric circulation (which is largely changing between seasons) plays an important role in IWV trends. Trends of opposite signs between winter and summer can be observed in western Antarctica, central South America, south Africa, eastern Europe and off the West coast of the USA. A strong drying occurs over Antarctica in JJA and over central Asia during JJA and DJF (though not exactly at the same location). Western Europe shows a drying in winter (DJF) and a moistening in summer, which explains the weak trend when considering the whole year. Over Australia, according to ERA-Interim, the drying is stronger in DJF, i.e. when associated with a decrease of the intensity of the moist flow during the monsoon period. The differences between our study and the one of Trenberth et al. (2005) are consistent with the theory that precipitation over western and northern Australia (the part of Australia mostly influenced by the monsoon flow in DJF) are strongly sensitive to the SST over the western central Pacific Ocean (10°S-10°N; 150°-200°E) (Brown et al., 2016). In ERA-Interim and Wang et al. (2016), during 1995-2010, the SST over this part of ocean has increased (indicated by a moistening, according to C-C law), and is associated with a drying over Australia, while during 1988-2001, a strong drying is observed over the central western Pacific Ocean, associated with a moistening over Australia. Another area likely sensitive to the intensity of the monsoon flow is northern Africa, where the drying is occurring in JJA over eastern Sahel, in a band covering Chad, Sudan and Eritrea. More details will be given in the discussion section.

Overall, the seasonal trends estimated from the GPS data are in good agreement with ERA-Interim and confirm the features discussed above. The sites with largest differences in the seasonal estimates are also listed in Table 2. In addition to the sites where issues were noticed in the monthly trends, the list includes a few more sites which also show up in Figs. 8a and b (most notably KIRU in Sweden, COCO in the Indian Ocean, IRKT in Russia, and ANKR in Turkey). Trend estimates at some of these sites might be inaccurate due to the enhanced impact of time gaps for the short seasonal time series (based on 16 years at best).

5 Trends in ERA-Interim and MERRA-2

5.1 Global analysis

In this section MERRA-2 is used to complement ERA-Interim and GPS namely in regions of high uncertainty in these datasets (e.g. Antarctica) or in regions where few or no GPS data are available (e.g. Africa, Asia, the global oceans). The monthly IWV trends computed for MERRA-2 (Figs. 9a, b) are in good agreement with ERA-Interim (Figs. 5a, b) for most of the regions. They describe consistent global moistening/drying dipoles along the inter-tropical Pacific Ocean, across Australia, South America and between eastern and western USA, and general moistening over the Arctic and Europe. However, there appears



to be also significant differences over several parts of the globe, in particular over Indonesia and the Indian Ocean, central Africa, western (coastal) and northern Africa, Central Asia and Antarctica.

Over Antarctica, the monthly trends in MERRA-2 (Figs. 9a, b) are significantly positive, in opposition to what is seen in ERA-Interim (Figs. 5a, b) where the trends are mainly negative, especially in the interior of the continent. However, one can notice
5 that ERA-Interim shows spotted areas of positive trends in the vicinity of the GPS stations which are in reasonable agreement with MERRA-2 and GPS. These locally positive trends in ERA-Interim might be explained by the influence of surface and/or upper air observations collected from these sites that are assimilated in this reanalysis. Comparing ERA-Interim and MERRA-2 IWV time series in the interior of the continent reveals that the reanalyses diverge mainly before year 2000, with a positive
10 trend in MERRA-2 between 1995 and 2000 (not shown). This divergence might be explained by a combination of differences in the observations actually assimilated and differences in the assimilation systems. Observations in the interior of the continent are most likely from satellites only. General documentation indicates that both reanalyses use the same types of satellite observations globally (Dee et al., 2011; Gelaro et al., 2017). However, it is not said whether or not these data are actually assimilated over Antarctica. This kind of information can only be checked from assimilation feedback statistics.

Over Indonesia and the Maritime Continent ERA-Interim trends are positive while MERRA-2 trends are negative. Comparing
15 IWV time series in the central part of this region reveals that though they are well correlated ($R=0.89$), MERRA-2 shows a larger seasonal cycle than ERA-Interim (not shown). GPS observations are only available at the outer bound of the domain where both reanalyses are in better agreement with each other and also with GPS except for station CCJM where GPS has a large discontinuity. Another exception is station GUAM (14°N , 145°E), where GPS is in good agreement with ERA-Interim while MERRA-2 has opposite trends. ERA-Interim and MERRA-2 trends also disagree in several places in central Asia,
20 namely in China where GPS data are in better agreement with MERRA-2 (stations WUHN and SHAO), and in northern and central Africa (but no GPS data are available there). The moistening trend over northern South America is seen in both reanalyses but is less intense in MERRA-2. However GPS trends at stations KOUR and BRAZ are in better agreement with ERA-Interim.

The seasonal trends computed from MERRA-2 (Figs. 9c, d) show quite good agreement with ERA-Interim and GPS in DJF
25 but much less in JJA. In DJF, the east-west dipole in the trends over Antarctica seen in ERA-Interim is confirmed by MERRA-2 (though the intensities are different), as well as the strong drying trend over Siberia, the Arabic peninsula, western Australia, western Europe, and most of the USA; and the strong moistening over the Arctic. In JJA, on the other hand, we can find many differences between the two reanalyses which were already noticed in the monthly trends. Opposite trends are seen in Indonesia and in most of south Asia, north and central Africa, Antarctica, but also in the eastern Arctic region.

30 Over Antarctica, the seasonal trends at the GPS stations are more consistent with MERRA-2 than with ERA-Interim in both seasons (Fig. 9c and d), though the GPS trends have a positive bias because of a processing inhomogeneity already mentioned. Interestingly, in JJA the contrasted trends with different signs seen in the GPS data (positive around SYOG, MAW1 and MCM4, and negative around DAV1 and CAS1) are well reproduced by MERRA-2, whereas the ERA-Interim trends are negative throughout.



Over Europe and Middle East, the contrasted trends between seasons seen in ERA-Interim (Fig. 5c and d) are confirmed with MERRA-2 (Fig. 9d and d) and are in accordance with GPS data at many sites, except at a few sites where GPS trends are opposite to both reanalyses, mainly: at KIRU (Sweden), IRKT (Russia), ANKR (Turkey). Opposite trends are also observed at other GPS sites over Scandinavia, namely at METS and SVTL (Finland) and ONSA (Sweden).

- 5 Over northern Africa, the two reanalyses show similar trend patterns in DJF, though not perfectly collocated (e.g. a tongue of negative trend is extending across western Sahel in ERA-Interim whereas in MERRA-2 it is more limited to the western countries: Senegal, Mauritania, and western Mali). In JJA, on the other hand, the strong drying already highlighted in ERA-Interim which extends over most of north Africa is almost absent in MERRA-2 where most of northern Africa is seen as moistening. This striking difference emphasizes the uncertainty of reanalyses in this data sparse region as also noticed by
- 10 Bauer, 2009, and Karbou et al., 2010.

Interpretation of IWV trends must be tempered by the fact that the time series used here are relatively short. Indeed, Trenberth et al. (2005) argued that the dominance of the 1997-98 El Niño event suggests that a longer time series may be required to obtain fully stable patterns of linear trends. The number of years needed to obtain a statistically significant trend in IWV in some regions, given its high variability, may never be achieved. In order to assess how consistent our trends obtained for the

15 1995-2010 period (when GPS data is available) are with longer-term trends, we computed them for the full length common to ERA-Interim and MERRA-2 (1980-2016).

On the monthly trends, most structures in ERA-Interim are similar for the short (Fig. 5a) and the long (Fig. 10a) period, although the intensities are weaker for the longer period (note that the colour bars are different for Figs. 5 and 10), but most of them are significant. Over land, the drying and moistening trends over Africa and South America show similar patterns, as

20 well as the moistening trends over eastern and northern regions of Europe and the drying trends over Antarctica. The main differences appear over the Arabic Peninsula, Western Australia, Mexico, and a small part of Antarctica. The drying trend over Australia observed for the shorter period is not observed in the long term. For this longer period, trends are mostly not statistically significant, which suggests that there might have been a moistening trend before the drying trend. Over the oceans, an overall moistening trend (except a strong drying off the coast of Antarctica) is observed, especially in the northern

25 hemisphere, but several areas show different patterns for both periods. For the Atlantic Ocean, a different sign is observed along the eastern coast of North America, with a significant moistening for the longer period, while a drying is confirmed by GPS around Bermuda for the shorter period. In the south, the drying trend is spatially more extended and statistically more significant for the longer period. Over the Indian ocean, for the short period, the western part moistens and the eastern part dries, and opposite trends are obtained over the longer period. Over the Pacific Ocean, even though the patterns look similar,

30 the spatial variability is stronger for the shorter period, with a more intense moistening along the equator, and west of Patagonia and a weaker moistening around Alaska.

Comparing the seasonal trends in ERA-Interim for both periods, the JJA patterns are mostly consistent over land and ocean between the two periods (Fig. 8b and Fig. 11f). Slight differences appear over India (where the moistening trend is more spatially extended in the longer period), Australia (where the trend is no longer significant), and Antarctica, where the drying



trend is shifted eastward. For DJF (Fig. 11b and Fig. 8a), stronger differences exist. While the moistening trend of the short period over northern South America, southern part of Africa, Central and northern Europe, western Canada and Alaska and Arctic are consistent with the longer period, the ones over Patagonia, part of China and Afghanistan, part of Antarctica and western Africa are no longer visible. The drying trends over Antarctica are extended to the entire continent for the longer period. The eastern USA that dries between 1995 and 2010 presents a moistening trend when considering the longer period. The strong drying obtained over Australia in DJF is mostly cancelled over the long period. Over the oceans, differences exist over the Indian Ocean, western Atlantic (along the east coast of USA), part of the south Atlantic and Pacific and mostly around Antarctica.

According to the Clausius-Clapeyron (C-C) equation, it is expected that an increasing temperature trend corresponds to an increasing IWV trend, especially over the oceans where the source of humidity is infinite. In order to assess the link between temperature and IWV trends, the trends in the 2-meter temperature were computed (even if the use of 2-m temperature may not be the best proxy of temperature in C-C equation). Monthly and globally (not shown), over the oceans, the temperature and water vapour trends have the same sign, despite some small-scale differences. Over land, all areas show an increase in T2m, except the high latitudes of the southern hemisphere. This means that, except over Antarctica, the drying observed in the afore-mentioned areas does not follow Clausius-Clapeyron relation. However, when we consider each season separately, some areas indicate a cooling (Figs. 11a, e) consistent with a drying (Figs. 11b, f). This is observed over Antarctica and to a lesser extent over Central Asia in DJF. Over eastern Australia, and South Africa, however, a weak cooling is observed while a significant moistening has been computed. For JJA, all continental areas show a significant warming, with the exception of parts of Antarctica, and a small area over northern Australia, where a cooling is also displayed, albeit not significant. Thus the C-C scaling ratio is not a good proxy for humidity when considering seasonal and regional variabilities and trends due to the important role of dynamics which allow the advection of dry or wet air masses (e.g. over USA, South America, eastern Sahel, and South Africa in JJA).

Trends in MERRA-2 over the long period (Fig. 11d, h) present different trends from ERA-Interim (Fig. 11b, f) over some areas as seen previously for the short period. They result from both the uncertainties that exist when computing trends, and from the differences in the physics and dynamics of the two reanalyses.

It is evident from Fig. 10 and 11 that MERRA-2 presents a more general moistening trend than ERA-Interim, especially in the southern hemisphere in DJF (Figs. 11b, d), and in both hemispheres in JJA (Figs. 11f, h). The main differences in the trends over oceans appear all around Antarctica, and those over continental areas are observed over Africa (where trends are positive in the North and negative in Central Africa in MERRA-2 and the opposite in ERA-Interim) and USA in JJA, over Australia in DJF and over Antarctica in both JJA and DJF. Over Africa and Antarctica, the important differences which exist between ERA-Interim and MERRA2 for both long and short term periods suggest that the physical processes are not well represented. These areas correspond to areas with very few observations available for data assimilation, reducing the constraint on the models. A more detailed investigation of the dynamics over Africa and Australia is presented in the following subsection.



Other regions, such as the Indo-Pacific region have different trends over the shorter period, but are in better agreement over the longer period. This is more obvious during JJA (although there are also differences in DJF) and can be explained by the strong variability that requires longer time series in order to obtain meaningful trends. The good agreement between reanalyses over this area is an important result regarding the fact that CMIP5 models have large biases over this region in present day Sea Surface Temperature, which has direct consequences on the future projection of precipitation over Australia (Brown et al., 2016; Grose et al., 2014). However, the link between IWV trends over these oceans and Australia is not that strong here, since over Australia, while reanalyses were in good agreement over the shorter period, the western part presents a significant moistening in MERRA-2 over the long period in DJF, and a weak and not statistically significant drying in ERA-Interim. This area is thus investigated in more details in the next subsection. This may suggest discontinuities in the reanalysis data (due to changes in the data assimilated) or an uncertainty in the computation of long-term trends (due to the presence of different shorter term trends during the longer period).

5.2 Analysis over Western Australia

Figure 12 displays the time series of IWV and temperature anomalies for a box over Western Australia (15-30°S, 115-135°E, as shown in Fig. 13) for both the short and long periods, for both the full time series and the DJF seasons. For the 1995-2010 period, both reanalyses show drying and warming monthly trends (Fig. 13b), with significant IWV trend in both while the temperature trend is only significant in ERA-Interim. For the longer time period (Fig. 13a), on the contrary, the monthly IWV trends are positive (moistening) for both reanalyses on average over the box, but not significant for ERA-Interim, and the temperature trends are again positive but smaller, and again significant for ERA-Interim. For DJF, the trends are generally consistent with the monthly trends, but of larger magnitude (e.g. IWV trends about $-2.4 \text{ kg m}^{-2} \text{ decade}^{-1}$ for the short period) though not statistically significant. It is noticeable that the difference in the IWV trends between reanalyses comes from the fact that ERA-Interim IWV starts with higher anomalies than MERRA-2 until 1990, but ends with lower anomalies after the late 2000s, so that the resulting trend is close to zero and not significant.

What is striking when looking at the full time series (Fig. 12a) is the existence of extreme cold and humid periods in both reanalyses after 1992, with a strong occurrence around the 2000s, which impact the linear trend estimate over the short period more strongly than over the long period. These periods correspond to DJF seasons 1997, 1999, 2000, 2001, 2006, and 2011 (Fig. 12c). Power et al. (1998) and Hendon et al. (2007) have shown that during DJF the correlation between wetter years and colder years is strong at interannual time scales. For the longer period, the correlation between T and IWV is around $r = -0.55$ for both reanalyses, while for the shorter period it is higher at $r = -0.78$ for ERA-Interim and $r = -0.73$ for MERRA-2. However, there is also a more complex interaction between temperature, IWV and precipitation in this region, with studies over Australia concluding that dynamics mostly explain the variability and trend of temperature and precipitation.

Consequently, we consider the wind at 925 hPa to assess the role of dynamics in these trends and variability. Figure 13 presents the mean zonal (u_{925}) and meridional (v_{925}) components of the wind, superposed by the trends of each component in contours. The mean states in u_{925} and v_{925} are similar in both reanalyses. The zonal components show mainly an easterly wind in the



latitude band between 30°S and 5°S throughout the year (Fig. 13a, b), slightly reduced at its northern border during DJF where the wind turns westerly (Fig. 13 e, f). The mean meridional component is southerly over Australia (Fig. 13c, d) with a changing direction at its northern border during DJF (Fig. 13 g, h) leading to a convergence within the box in DJF. The convergence is roughly from north-east in the northern part of the box and from south-east in the southern part.

- 5 The trends show a reinforcement of the mean easterly component in the box in both reanalyses (Fig. 13a, b). In DJF, the easterly flow in ERA-Interim is increasing at the eastern border of the box and over central Australia while it is decreasing at the western border and over eastern Indian Ocean, hence explaining at least partly the drying and warming trend over the box (Fig. 12d). The trends in the mean meridional component are positive though quite weak in both reanalyses (Fig. 13c, d), thus indicating a strengthening of the mean southerly flow. During DJF, the meridional trend is very small in ERA-Interim while
- 10 it is slightly positive again in MERRA-2.

Figure 14 displays the time series of wind vectors over the same box as Fig. 13. Figure 14a shows that the mean wind direction does not change much over the year, though the strength is slightly larger in the summer season (from January to March) due to an increase in the easterly component. The interannual variability is quite marked, both in DJF (Fig. 14b) and JJA (Fig. 14c). It is clear that the anomalously moister summers seen in Fig. 12 are associated with a dynamical anomaly, with a weaker

15 wind, and a direction switching from south-easterly to easterly. The amplitude of wind direction difference is stronger in MERRA-2 than in ERA-Interim but both reanalyses are consistent.

5.3 Analysis over North Africa/eastern Sahel

Here we focus on a box over the eastern Sahel (10-20°N, 10-40°E). The monthly trend in IWV is negative (drying) and significant in both reanalyses, though it is twice as intense in ERA-Interim than in MERRA-2 (Fig. 15b). Similarly, the

20 temperature trends are positive (warming) and significant in both reanalyses. Over the long period, the IWV trend in MERRA-2 is close to zero and not significant while that of ERA-Interim is still significantly negative, while the temperature trends are again positive (Fig. 15a). Though the monthly anomalies show many similarities, their agreement is not as good as seen for the box over Australia. The general strong negative IWV trend in ERA-Interim implies that IWV anomalies are higher in ERA-Interim at the beginning of the period and lower at the end of the period. However, both reanalyses present four different

25 periods in the time IWV series: a drying trend at the very beginning (1980-1985) followed by a moistening trend until 1995, then followed by a new drying period lasting until around 2008 when the trend seems to stop. As a consequence, over the shorter period, both reanalyses show a significant monthly drying, even though for ERA-Interim the IWV trend is twice as intense (Fig. 15b).

As observed for IWV anomalies, the trend in T anomalies stops at around 2008 (Fig. 15a). Before that period, the temperature

30 anomaly is increasing significantly, despite strong month-to-month variability. However, low correlation appears between IWV and T anomalies when considering full time series (Fig. 15a). For the longer period, the correlation between T and IWV is close to zero for MERRA-2 and about $r = -0.31$ for ERA-Interim, while for the shorter period it is higher at $r = -0.41$ for ERA-Interim and $r = -0.29$ for MERRA-2. In JJA, the trends are strong and go on after 2008 (Fig. 15c). The correlation of



anomalies for JJA between both reanalyses is quite good, both for IWV (around $r = 0.67$ for the short period and $r = 0.63$ for the longer period) and T (around $r = 0.69$ for both periods), although their amplitudes and trends are quite different. MERRA-2 presents an overall moistening trend in JJA over the long period, while ERA-Interim shows a drying (Fig. 15c). IWV trends in both reanalyses are significant but of opposite signs, while the temperature trends are both positive and significant. Over the short period (Fig. 15d), the IWV trend in MERRA-2 becomes close to zero while the other trends remain consistent with the longer period. Over the short period, the IWV trend in JJA in MERRA-2 is close to zero while it is still strongly negative in ERA-Interim (Fig. 15d). The relation between IWV and temperature trends in this arid region is not expected to follow C-C relationship and IWV especially is expected to be more related to changes in the atmospheric circulation.

The zonal and meridional wind components at 925hPa over the short period are shown in Fig. 16. The mean states are plotted in colours over which the contours of the trends are superposed. The mean states in u_{925} and v_{925} are similar in both reanalyses, with a mean monthly north-easterly wind over the box (Fig. 16a, b, c, d) which is almost completely replaced with a south-westerly wind in JJA (Fig. 16e, f, g, h). This wind is slightly stronger in ERA-Interim than in MERRA-2. For both reanalyses, the trends in the mean flow indicate an increase in the zonal component (Fig. 16a, b). The trends in the meridional wind component show a dominant increase in the northerly from the Sahara. This trend may explain the general warming and drying in the eastern Sahel. The trends differ, however, with MERRA-2 showing a decrease in the northerly flow in upper-left angle of the box (Fig. 16d) while ERA-Interim shows an increase there and an increasing southerly inflow at the southern border of the box (Fig. 16c). This difference can explain the difference of intensity in these trends. In JJA, the trends in MERRA-2 are very weak (Fig. 16f, h) while in ERA-Interim there is a strong increasing of the southerly flow from the Central Africa and of the north-easterly flow from the Sahara, explaining the net drying and warming (Fig. 15d).

The monthly mean time series of the wind in the box (Fig. 17a) clearly indicates the time of the monsoon onset (May), when the wind shifts from north-easterly to south-westerly and retreat (September). This monsoon flow appears stronger in ERA-Interim than in MERRA-2, while the dry season flow is stronger in MERRA-2 (see also Fig. 17b and c). From the time series of JJA wind vectors (Fig. 17b) it is clear that ERA-Interim has a stronger southerly flow with large interannual and decadal variability. The time series of wind in JJA in MERRA-2 clearly indicates the same four periods than for the IWV trends identified above, with a weakening of the south-westerly wind between 1980 and 1985, followed by an intensification of the monsoon flow arriving in this box between 1985 and 1995, and a wind decreasing and turning to the west until 2005 or 2006 and then becoming more stable on average. In ERA-Interim, we only observe two main periods: a weaker south/south-westerly wind at the beginning of the period followed by an intensification after 1990. The wind intensity is maximum between 1995 and 2000 but stays quite intense and with a south/south-westerly direction until the end of the period, being stronger and more southerly than in MERRA-2 after 2000. The different dynamics of the two reanalyses observed in this box partly explains the increasing deviation between both reanalyses at the end of the period.



6 Summary

- In this paper we used IWV data from GPS observations and reanalyses (ERA-Interim and MERRA-2) to study water vapour trends and variability for the 1995-2010 period mainly. We found that the means and variability are well represented in ERA-Interim compared to GPS, even in regions of high IWV gradients. Some differences were pointed out between GPS and ERA-Interim at certain stations. These sites are mostly located in coastal regions and regions of complex topography. Representativeness errors are the main suspected cause, due to the large variations in the IWV and altitude from ERA-Interim at the grid points surrounding the GPS station, or the large height differences between the model surface and the GPS antenna. These GPS stations might be useful to study local atmospheric processes but are not as much representative of larger scale IWV variations.
- Next, the GPS data and both reanalyses were used to study the trends in IWV over the period 1995-2010. Strong monthly trends were found in both reanalyses. First, in ERA-Interim, significant moistening trends were observed over most of the tropical oceans and over the Arctic, while significant drying was observed in south-tropical eastern Pacific region, west of the United States and generally south of 60°S. Over land, significant positive trends were observed in northern South America, Central Africa, and Indonesia, over northern North America, Greenland, most of Europe and Siberia. Significant negative trends over land were observed over North Africa, Australia, Antarctica, central Asia, and most of the USA. These trends were compared with GPS and were found to be in general good agreement, but with opposite sign trend at some sites. Discrepancies at most of these sites were found to be due to gaps in the GPS time series (when time-matched series are compared, the agreement is improved) and discontinuities (some of which explained by reported GPS equipment changes), but drifts in the ERA-Interim reanalysis are also plausible.
- The seasonal trends (for DJF and JJA) presented stronger absolute and relative trends. In some regions, trends can have opposite signs in winter and summer, which emphasizes the role of atmospheric circulation in IWV trends. The comparison of ERA-Interim and GPS seasonal trends is consistent with the monthly trends. However, the differences are generally of larger magnitudes and a few more sites show trends with opposite signs. This is mainly due to the enhanced impact of time gaps for the short seasonal time series.
- The results for MERRA-2 appear to be different from ERA-Interim over several parts of the globe, in particular over Indonesia and Indian Ocean, central Africa, Western (coastal) and Northern Africa, Central Asia and Antarctica (where there appears to be some uncertainty in all datasets). The trends for 1995-2010 were also compared with longer-term trends, for the 1980-2016 period. For both long and short term periods, important differences were found between ERA-Interim and MERRA2 over Africa and Antarctica. These areas correspond to areas with very few observations available for data assimilation, which suggest that some physical processes (e.g. dry convection involved in the Saharan heat low) might not be well represented. A more detailed investigation of the dynamics over the eastern Sahel in north Africa and western Australia was presented. We considered the wind at 925 hPa to assess the role of dynamics in the IWV and temperature trends and variability. Anomalies



in the wind speed and direction were associated with differences in IWV anomalies, and differences in the winds for both reanalyses were found to enhance the differences in IWV trends.

Acknowledgements. This work was developed in the framework of the VEGA project and supported by the CNRS program LEFE/INSU and ANR REMEMBER project (grant ANR-12-SENV-001). This work is a contribution to the European COST
5 Action ES1206 GNSS4SWEC (GNSS for Severe Weather and Climate monitoring; http://www.cost.eu/COST_Actions/essem/ES1206) aiming at the development of the global GPS network for atmospheric research and climate change monitoring.

References

- Barnston, A. G., and Livezey, R. E.: Classification, seasonality and persistence of low-frequency atmospheric circulation
10 patterns, *Mon. Weather Rev.*, 115(6), 1083-1126, doi: 10.1175/1520-0493(1987)115<1083:CSAPOL>2.0.CO;2, 1987.
- Bastin, S., Bock, O., Chiriaco, M., Drobinski, P., Roehrig, R., Ahrens, B., Gallardo, C., Dominguez-Alonso, M., and Li, L.:
Evaluating the impact of humidity bias on light precipitation estimates in Med-CORDEX/Hymex simulations using long term
GPS network and ground-based datasets, Submitted to *Atmos. Chem. Phys. special issue*.
- Bauer, P.: 4D-Var assimilation of MERIS total column water-vapour retrievals over land, *Q. J. Roy. Meteor. Soc.*, 135: 1852–
15 1862, doi:10.1002/qj.509, 2009.
- Bengtsson, L., Hagemann, S., and Hodges, K. I.: Can climate trends be calculated from reanalysis data?, *J. Geophys. Res.*
Atmos., 109(D11), doi: 10.1029/2004JD004536, 2004.
- Bock, O., Bouin, M. N., Walpersdorf, A., Lafore, J. P., Janicot, S., and Guichard, F.: Comparison of GPS precipitable water
vapour to independent observations and Numerical Weather Prediction model reanalyses over Africa, *Q. J. Roy. Meteor. Soc.*,
20 133, 2011-2027, doi: 10.1002/qj.185, 2007.
- Bock, O., Willis, P., Wang, J., and Mears, C.: A high-quality, homogenized, global, long-term (1993–2008) DORIS
precipitable water data set for climate monitoring and model verification, *J. Geophys. Res. Atmos.*, 119(12), 7209-7230, doi:
10.1002/2013JD021124, 2014.
- Bock, O., Bossler, P., Pacione, R., Nuret, M., Fourrié, N., and Parracho, A.: A high-quality reprocessed ground-based GPS
25 dataset for atmospheric process studies, radiosonde and model evaluation, and reanalysis of HyMeX Special Observing Period,
Q. J. Roy. Meteor. Soc., 142(S1), 56-71, doi: 10.1002/qj.2701, 2016.
- Brown, J. R., Moise, A. F., Colman, R., and Zhang, H.: Will a Warmer World Mean a Wetter or Drier Australian Monsoon?,
J. Climate, 29(12), 4577-4596, doi: 10.1175/JCLI-D-15-0695.1, 2016.
- Byun, S.H. and Bar-Server, Y. E.: A new type of troposphere zenith path delay product of the international GNSS service, *J.*
30 *Geodesy*, 83(3-4), 367-373, doi: 10.1007/s00190-008-0288-8, 2009.



- Collins, M., An, S.I., Cai, W., Ganachaud, A., Guilyardi, E., Jin, F.F., Jochum, M., Lengaigne, M., Power, S., Timmermann, A., and Vecchi, G.: The impact of global warming on the tropical Pacific Ocean and El Nino, *Nat. Geosci.*, 3, 391-397, doi:10.1038/ngeo868, 2010.
- Collins, M., An, S.I., Cai, W., Ganachaud, A., Guilyardi, E., Jin, F.F., Jochum, M., Lengaigne, M., Power, S., Timmermann, A., and Vecchi, G.: The impact of global warming on the tropical Pacific Ocean and El Niño, *Nat. Geosci.*, 3(6), 391-397, doi:10.1038/ngeo868, 2010.
- Dee, D.P., Uppala, S.M., Simmons, A.J., Berrisford, P., Poli, P., Kobayashi, S., Andrae, U., Balmaseda, M.A., Balsamo, G., Bauer, P., and Bechtold, P.: The ERA-Interim reanalysis: Configuration and performance of the data assimilation system, *Q. J. Roy. Meteor. Soc.*, 137(656), 553-597, doi: 10.1002/qj.828, 2011.
- Dessler, A. E., and Davis, S. M.: Trends in tropospheric humidity from reanalysis systems, *J. Geophys. Res. Atmos.*, 115, D19127, doi: 10.1029/2010JD014192, 2010.
- Gelaro, R., McCarty, W., Suárez, M.J., Todling, R., Molod, A., Takacs, L., Randles, C.A., Darmenov, A., Bosilovich, M.G., Reichle, R., and Wargan, K.: The modern-era retrospective analysis for research and applications, version 2 (MERRA-2), *J. Climate*, 30(14), 5419-5454, doi: 10.1175/JCLI-D-16-0758.1, 2017.
- Hamed, K. H., and Rao, A. R.: A modified Mann-Kendall trend test for autocorrelated data, *J. Hydrol.*, 204(1-4), 182-196, doi: 10.1016/S0022-1694(97)00125-X, 1998.
- Held, I. M., and Soden, B. J.: Robust responses of the hydrological cycle to global warming, *J. Climate*, 19(21), 5686-5699, doi: 10.1175/JCLI3990.1, 2006.
- Hendon, H. H., Thompson, D. W. J., Wheeler, and M. C.: Australian Rainfall and Surface Temperature Variations Associated with the Southern Hemisphere Annular Mode, *J. Climate*, Vol. 20 Issue 11, p2452-2467, doi: 10.1175/JCLI4134.1, 2007.
- Holloway, C. E. and Neelin, J. D.: Moisture vertical structure, column water vapour, and tropical deep convection, *J. Atmos. Sci.*, 66(6), 1665-1683, doi: 10.1175/2008JAS2806.1, 2009.
- IGSMail-6298, Reprocessed IGS Trop Product now available with Gradients, by Yoaz Bar-Sever, 11 Nov 2012, <http://igs.cb.jpl.nasa.gov/pipermail/igsmail/2010/007488.html>.
- Karbou, F., Rabier, F., Lafore, J.-P., Redelsperger, J. L., and Bock, O.: Global 4D-Var assimilation and forecast experiments using land surface emissivities from AMSU-A and AMSU-B. Part-II: Impact of adding surface channels on the African Monsoon during AMMA, *Weather Forecast*, 25, 20-36, doi:10.1175/2009WAF2222244.1, 2010.
- King, A., Donat, M., Alexander, L., and Karoly, D.: The ENSO-Australian rainfall teleconnection in reanalysis and CMIP5, *Clim. Dynam.*, Vol. 44 Issue 9/10, 2623-2635, doi: 10.1007/s00382-014-2159-8, 2015.
- Kondratiev, K. Y.: *Radiation Processes in the Atmosphere* (Geneva: World Meteorological Organization), 1972.
- Lorenz, D. J. and DeWeaver, E. T.: Tropopause height and zonal wind response to global warming in the IPCC scenario integrations, *J. Geophys. Res. Atmos.*, 112(D10119), doi: 10.1029/2006JD008087, 2007.
- Lorenz, A. C.: Analysis methods for numerical weather prediction, *Q. J. Roy. Meteor. Soc.*, 112: 1177-1194, doi:10.1002/qj.49711247414, 1986.



- Mieruch, S., Schröder, M., Noël, S., and Schulz, J.: Comparison of decadal global water vapour changes derived from independent satellite time series, *J. Geophys. Res. Atmos.*, 119(22), 12489-12499, doi: 10.1002/2014JD021588, 2014.
- Neelin, J. D., Peters, O., and Hales, K.: The transition to strong convection, *J. Atmos. Sci.*, 66(8), 2367-2384, doi: 10.1175/2009JAS2962.1, 2009.
- 5 Ning, T., Wickert, J., Deng, Z., Heise, S., Dick, G., Vey, S., and Schöne, T.: Homogenized time series of the atmospheric water vapour content obtained from the GNSS reprocessed data, *J. Climate*, 29(7), 2443-2456, doi: 10.1175/JCLI-D-15-0158.1, 2016.
- Power, S., Tseitkin, F., Torok, S., Lavery, B., and McAvaney, B.: Australian temperature, Australian rainfall, and the Southern Oscillation, 1910–1996: Coherent variability and recent changes, *Aust. Meteorol. Mag.*, 47, 85–101, 1998.
- 10 Ross, R. J. and Elliott, W. P.: Tropospheric water vapour climatology and trends over North America: 1973–93, *J. Climate*, 9(12), 3561-3574, doi:10.1175/1520-0442(1996)009<3561:TWVCAT>2.0.CO;2, 1996.
- Ross, R. J. and Elliott, W. P.: Radiosonde-based Northern Hemisphere tropospheric water vapour trends, *J. Climate*, 14(7), 1602-1612, doi:10.1175/1520-0442(2001)014<1602:RBNHTW>2.0.CO;2, 2001. d
- Rousseeuw, P. J. and Leroy, A. M.: Robust Regression and Outlier Detection, Wiley Series in Probability and Mathematical
15 Statistics, 516, Wiley, p. 67, 2003. ISBN 978-0-471-48855-2.
- Ruti, P.M., Somot, S., Giorgi, F., Dubois, C., Flaouanas, E., Obermann, A., Dell'Aquila, A., Pisacane, G., Harzallah, A., Lombardi, E., and Ahrens, B.: MED-CORDEX initiative for Mediterranean climate studies, *B. Am. Meteorol. Soc.*, 97(7), 1187-1208, doi: 10.1175/BAMS-D-14-00176.1, 2016.
- Sahany, S., Neelin, J. D., Hales, K., and Neale, R. B.: Temperature–moisture dependence of the deep convective transition as
20 a constraint on entrainment in climate models, *J. Atmos. Sci.*, 69(4), 1340-1358, doi: 10.1175/JAS-D-11-0164.1, 2012.
- Schröder, M., Lockhoff, M., Forsythe, J. M., Cronk, H. Q., Vonder Haar, T. H., and Bennartz, R.: The GEWEX Water Vapour Assessment: Results from Intercomparison, Trend, and Homogeneity Analysis of Total Column Water Vapour, *J. Appl. Meteorol. Clim.*, 55(7), 1633-1649, doi: 10.1175/JAMC-D-15-0304.1, 2016.
- Semenov, V. and Bengtsson, L.: Secular trends in daily precipitation characteristics: greenhouse gas simulation with a coupled
25 AOGCM, *Clim. Dynam.*, 19(2), 123-140, doi: 10.1007/s00382-001-0218-4, 2002.
- Sen, P. K.: Estimates of the regression coefficient based on Kendall's tau, *J. Am. Stat. Assoc.*, 63 (324): 1379–1389, JSTOR 2285891, MR 0258201, doi:10.2307/2285891, 1968.
- Theil, H.: A rank-invariant method of linear and polynomial regression analysis, I, II, III, *Nederl. Akad. Wetensch., Proc.*, 53: 386–392, 521–525, 1397–1412, MR 0036489, doi: 10.1007/978-94-011-2546-8_20, 1950.
- 30 Trenberth, K. E., Fasullo, J., and Smith, L.: Trends and variability in column-integrated atmospheric water vapour, *Clim. Dynam.*, 24(7-8), 741-758, doi: 10.1007/s00382-005-0017-4, 2005.
- Trenberth, K. E., Smith, L., Qian, T., Dai, A., and Fasullo, J.: Estimates of the global water budget and its annual cycle using observational and model data, *J. Hydrometeorol.*, 8(4), 758-769, doi: 10.1175/JHM600.1, 2007.



- Vey, S., Dietrich, R., Fritsche, M., Rülke, A., Steigenberger, P., and Rothacher, M.: On the homogeneity and interpretation of precipitable water time series derived from global GPS observations, *J. Geophys. Res. Atmos.*, 114, D10101, doi: 10.1029/2008JD010415, 2009.
- Wagner, T., Beirle, S., Grzegorski, M., and Platt, U.: Global trends (1996–2003) of total column precipitable water observed by Global Ozone Monitoring Experiment (GOME) on ERS-2 and their relation to near-surface temperature, *J. Geophys. Res. Atmos.*, 111, D12102, doi: 10.1029/2005JD006523, 2006.
- Wang, J., Zhang, L., and Dai A.: Global estimates of water-vapour-weighted mean temperature of the atmosphere for GPS applications, *J. Geophys. Res.*, 110, D21101, doi:10.1029/2005JD006215, 2005.
- Wang, J., Dai, A., and Mears, C.: Global Water Vapour Trend from 1988 to 2011 and Its Diurnal Asymmetry Based on GPS, Radiosonde, and Microwave Satellite Measurements, *J. Climate*, 29(14), 5205-5222, doi: 10.1175/JCLI-D-15-0485.1, 2016.
- Wardle, R. and Smith, I.: Modeled response of the Australian monsoon to changes in land surface temperatures, *Geophys. Res. Lett.*, 31, L16205, doi:10.1029/2004GL020157, 2004.
- Wolter, K., and Timlin, M. S.: Monitoring ENSO in COADS with a seasonally adjusted principal component index, In Proc. of the 17th Climate Diagnostics Workshop (Vol. 5257), 1993.
- Wolter, K., and Timlin, M. S.: Measuring the strength of ENSO events: How does 1997/98 rank?, *Weather*, 53(9), 315-324, doi: 10.1002/j.1477-8696.1998.tb06408.x, 1998.


Table 1: Statistics (median \pm one standard deviation over 104 stations) of differences (ERA-Interim minus GPS) of mean IWV values and of relative standard deviations.

| | Diff. of mean IWV (ERA-Interim – GPS) | Diff. of rel. std. (ERA-Interim – GPS) |
|------------|--|--|
| DJF | +0.51 kg.m ⁻² \pm 0.83 kg.m ⁻² +6.2% \pm 6.9% | -0.05% \pm 1.69% |
| JJA | +0.52 kg.m ⁻² \pm 0.95 kg.m ⁻² +2.7% \pm 7.8% | -0.15% \pm 4.07% |

5 Table 2: Stations with most intense trend differences (ERA-Interim – GPS) computed from time-matched GPS and ERA-Interim IWV series.

| | Full time series | DJF | JJA |
|---|------------------------|------------------------------------|------------------------------------|
| Tr.diff < -1 kg.m ⁻² .decade ⁻¹ | WUHN, CRO1, CFAG, SHAO | WUHN, PIN1 | WUHN, SHAO, CRO1, CFAG, KOUR, WSLR |
| Tr.diff > 1 kg.m ⁻² .decade ⁻¹ | CCJM | CCJM, DARW, GUAM, LPGS, COCO, SANT | CCJM, POL2 |
| Tr.diff < -7 %.decade ⁻¹ (*) | MCM4, MAW1, PIN1 | IRKT, POL2, PIN1, WUHN, YELL, WSLR | MCM4, MAW1, SYOG |
| Tr.diff > 7%.decade ⁻¹ (*) | CCJM | CCJM, KIRU | AREQ |

 (*) for the seasonal trends, the threshold on trend difference is 10%.decade⁻¹

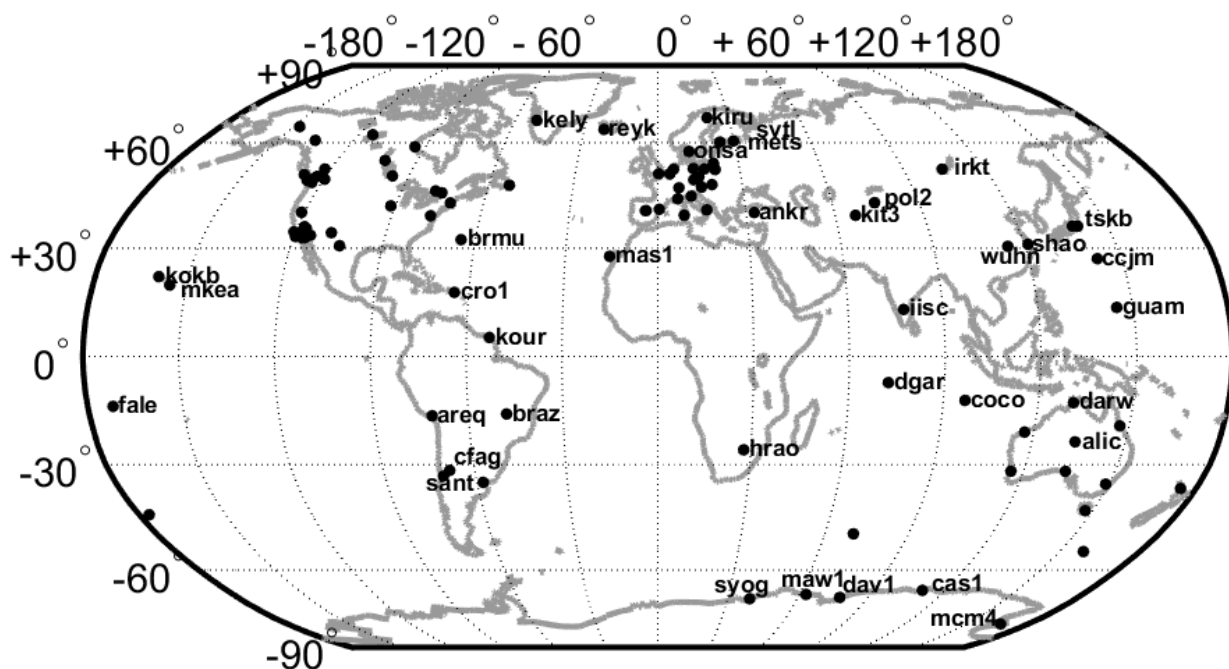


Figure 1: Map showing the 104 GPS stations used in this study. The stations discussed in the text are identified by their 4-character ID.

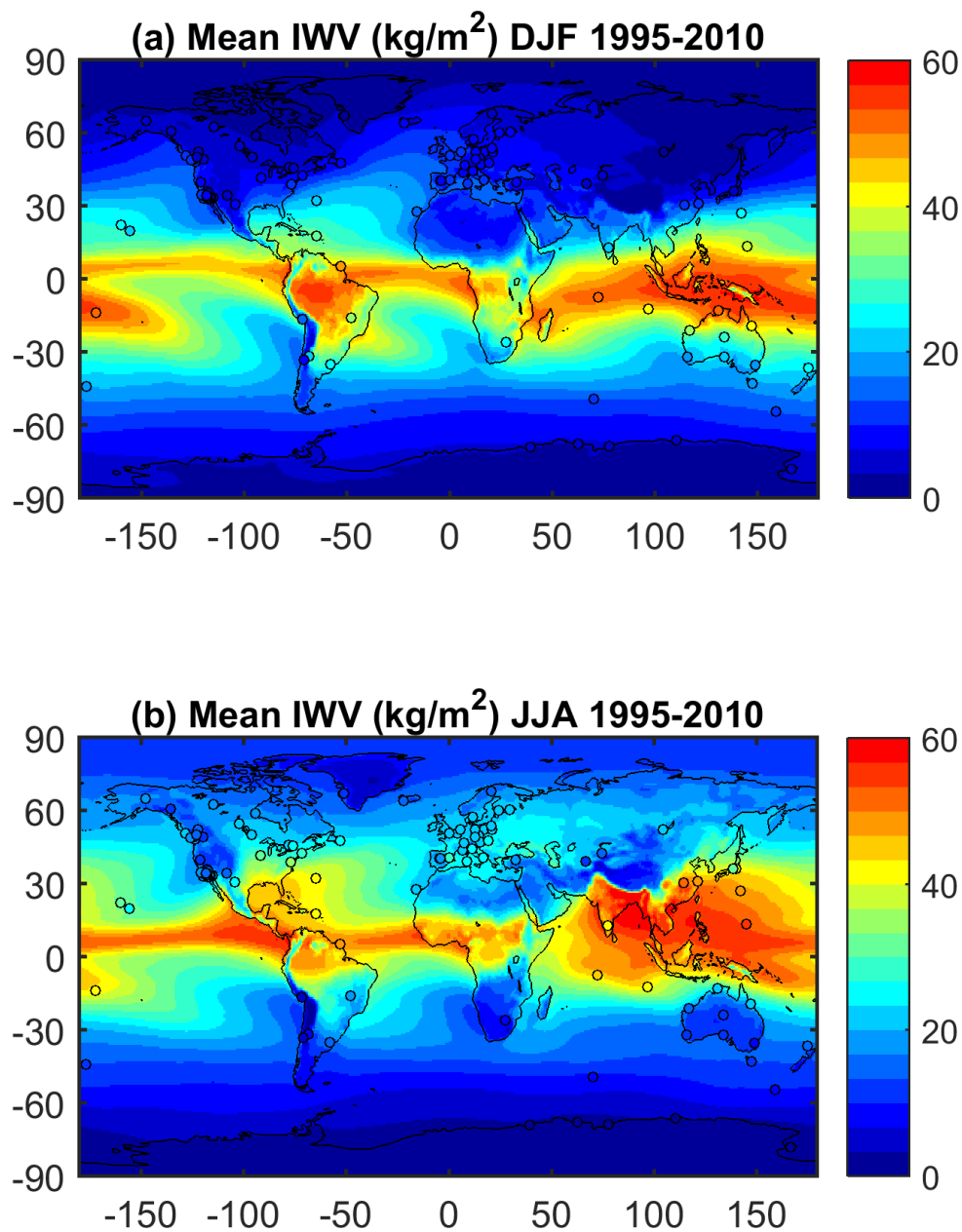


Figure 2: (a) Mean I WV for DJF 1995-2010 from ERA-Interim (shading) and GPS (filled circles), (b) same as (a) for JJA.

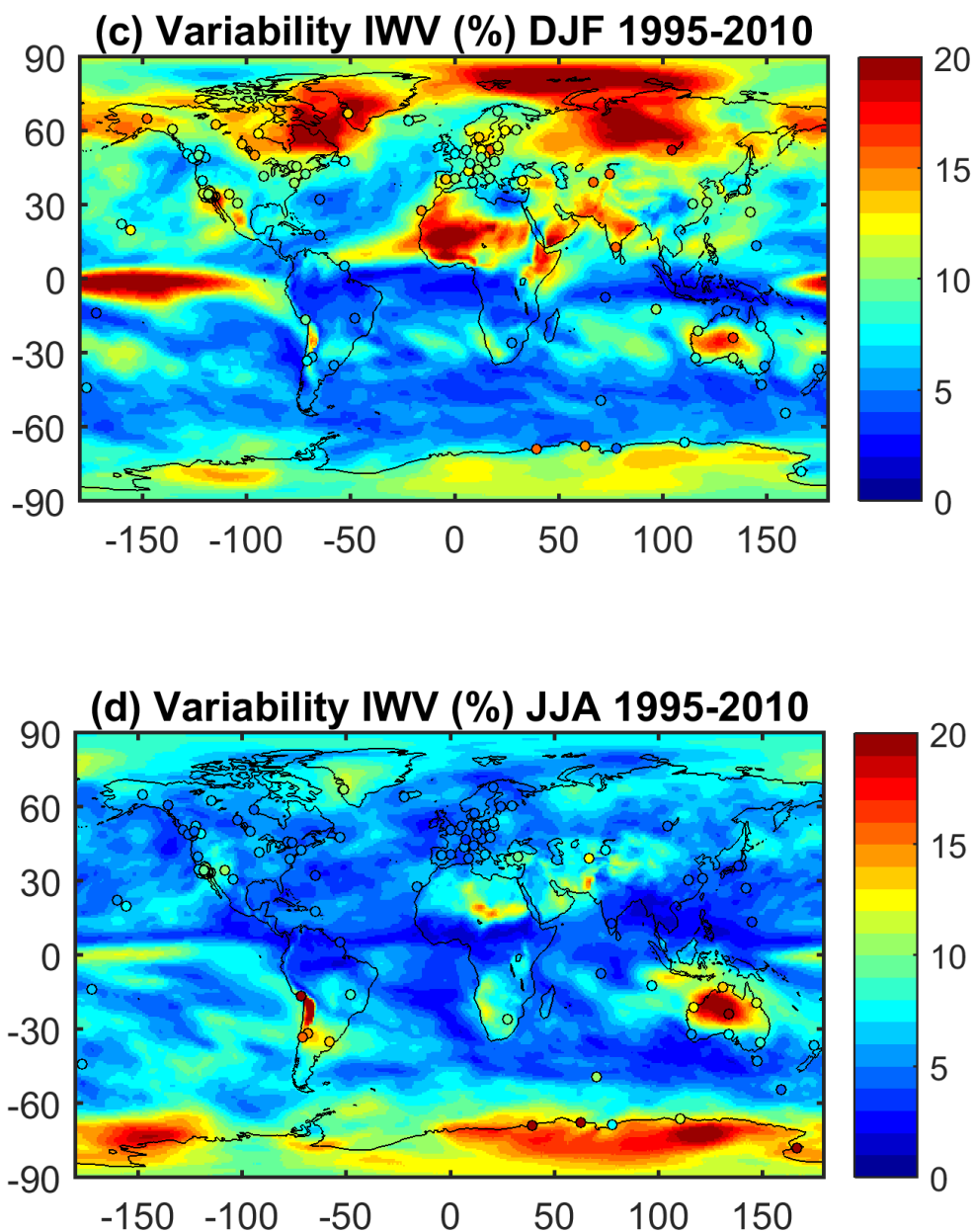
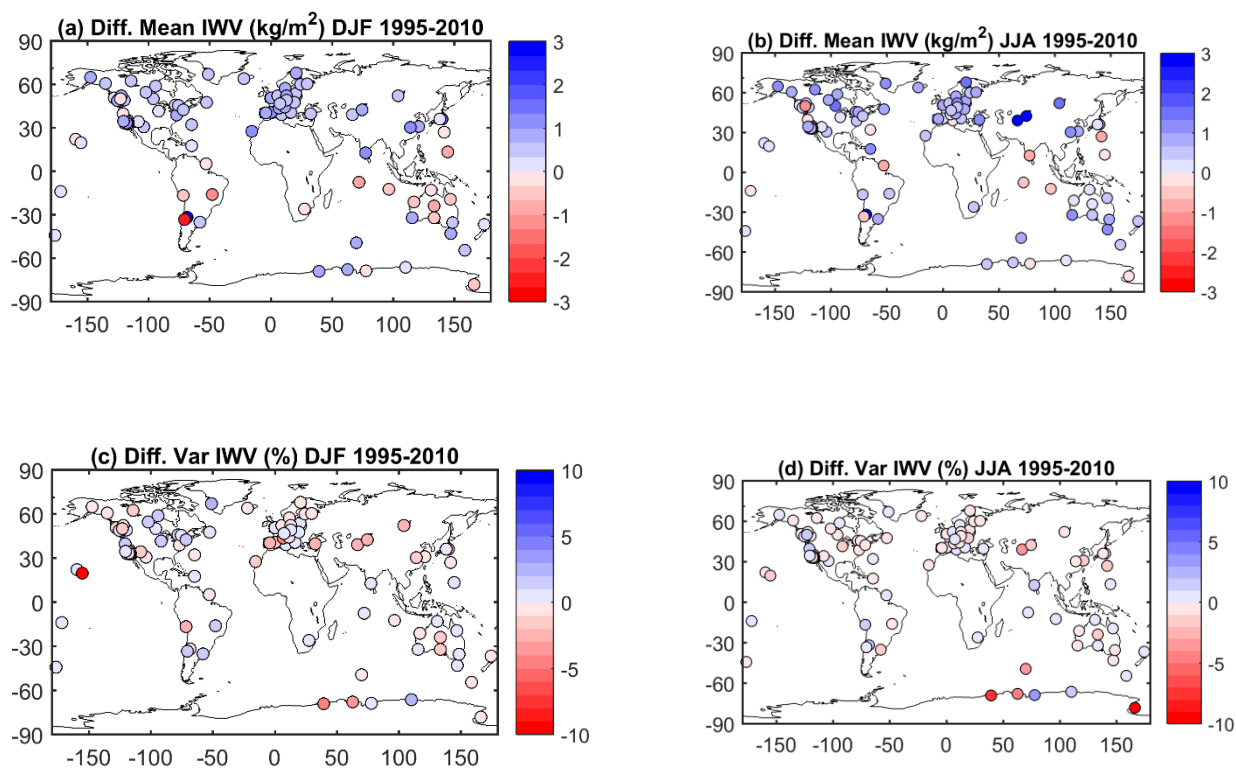


Figure 2 (continued): (c) Relative variability in % (standard deviation of the IWV series divided by its mean) for DJF 1995-2010, (d) Same as (c) for JJA.



5 **Figure 3:** (a) Difference of mean IWV estimates (ERA-Interim minus GPS) for DJF 1995-2010 from time-matched IWV series, (b) same as (a) for JJA, (c) difference of relative variability estimates (ERA-Interim variability minus GPS variability) for DJF 1995-2010 from time-matched IWV series, (d) same as (c) for JJA.

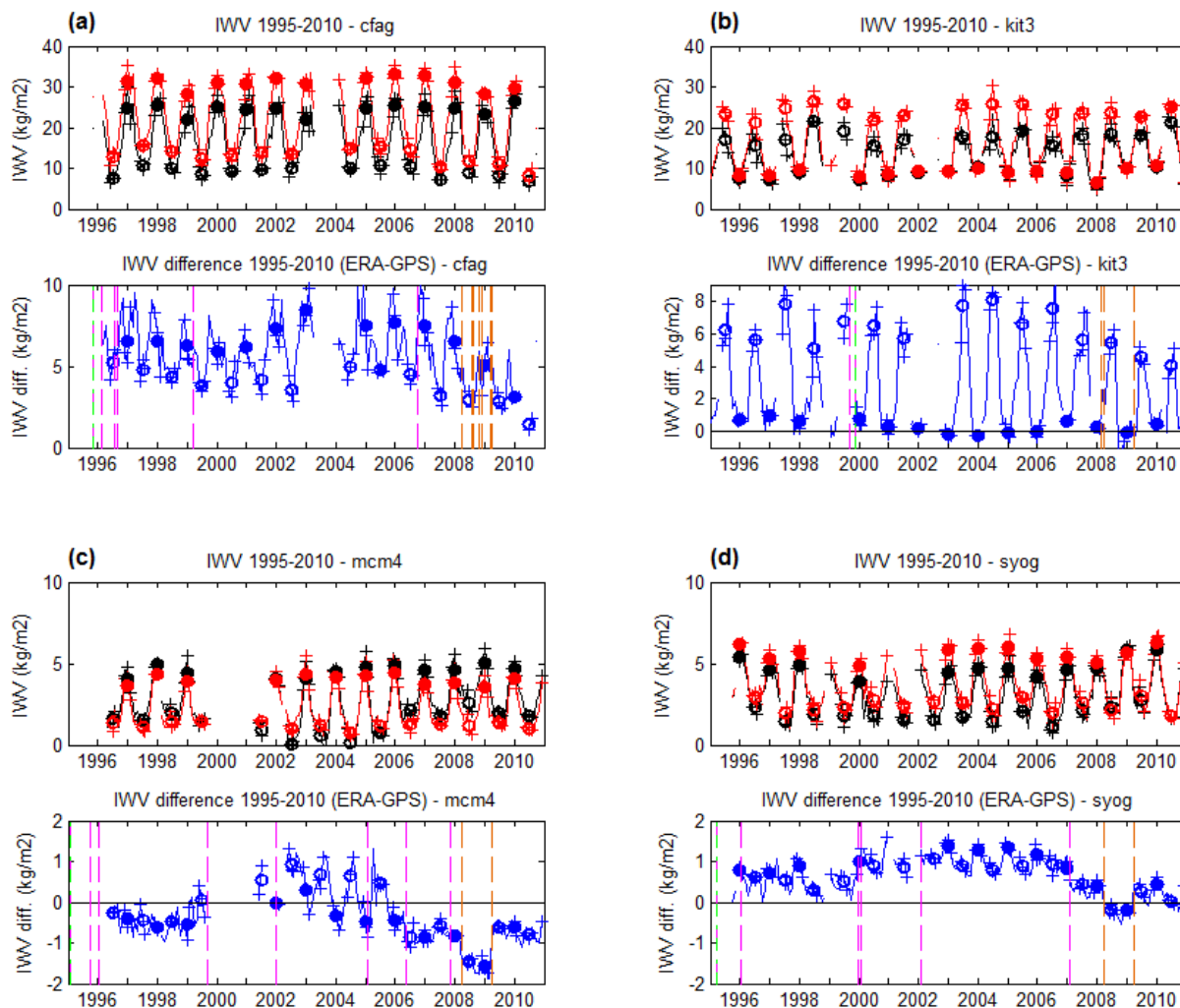
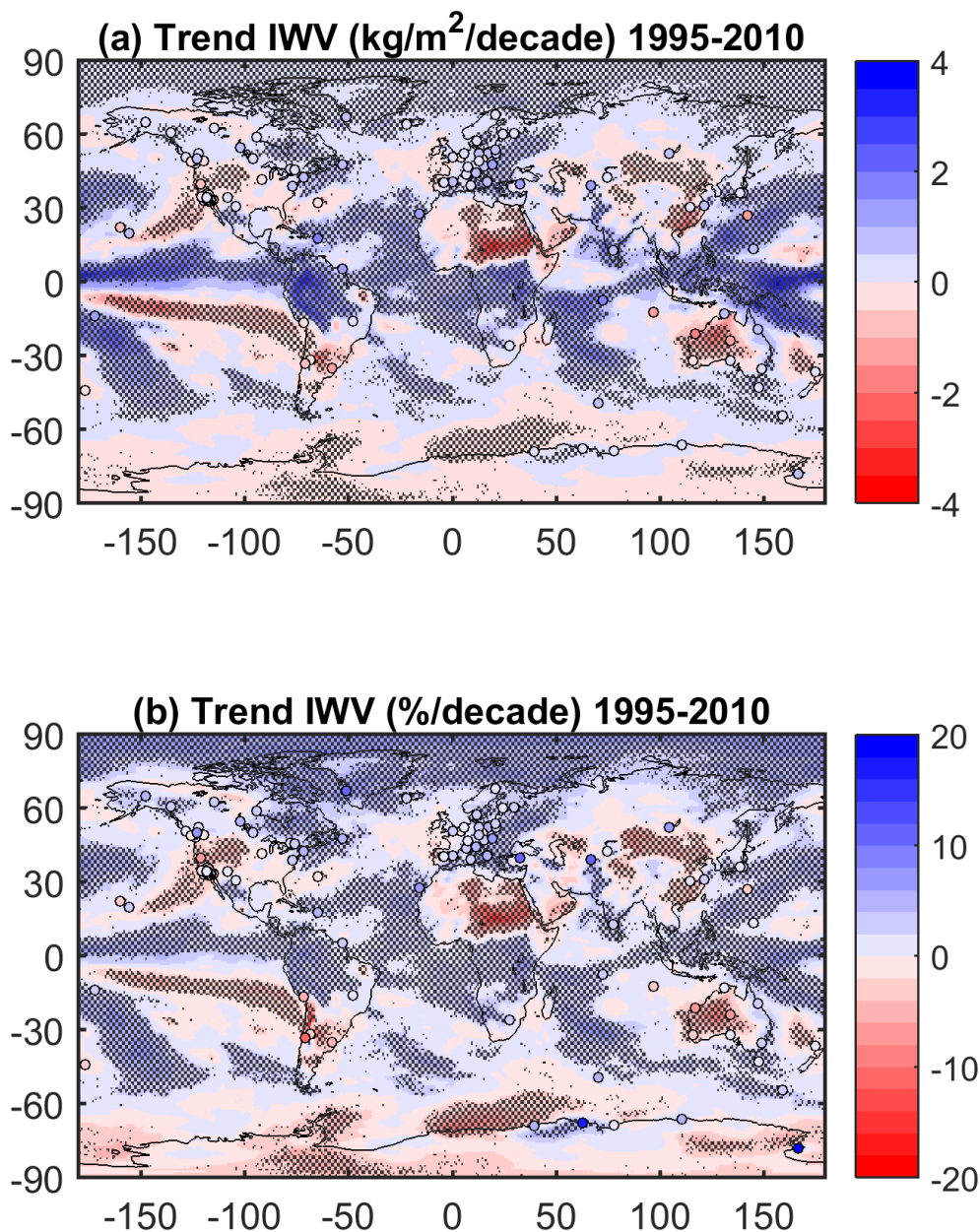


Figure 4: Time series of IWV from GPS (black) and ERAI (red), and IWV difference (blue) at stations (a) CFAG, (b) KIT3, (c) MCM4 and (d) SYOG. Filled circles show the DJF values and open circles the JJA values. Crosses show the individual months used in both seasons. Vertical dashed lines indicate GPS equipment changes (receiver in magenta, antenna in green) and GPS processing changes (in orange). Note the change in vertical scales between figures.

5



5 **Figure 5: Absolute (a) and relative (b) IWV trends for the 1995-2010 period from ERA-Interim and GPS (stations marked as circles). The statistically significant trends from ERA-Interim are highlighted by stippling. Absolute trends are in kg/m^2 per decade and relative trends in % per decade.**

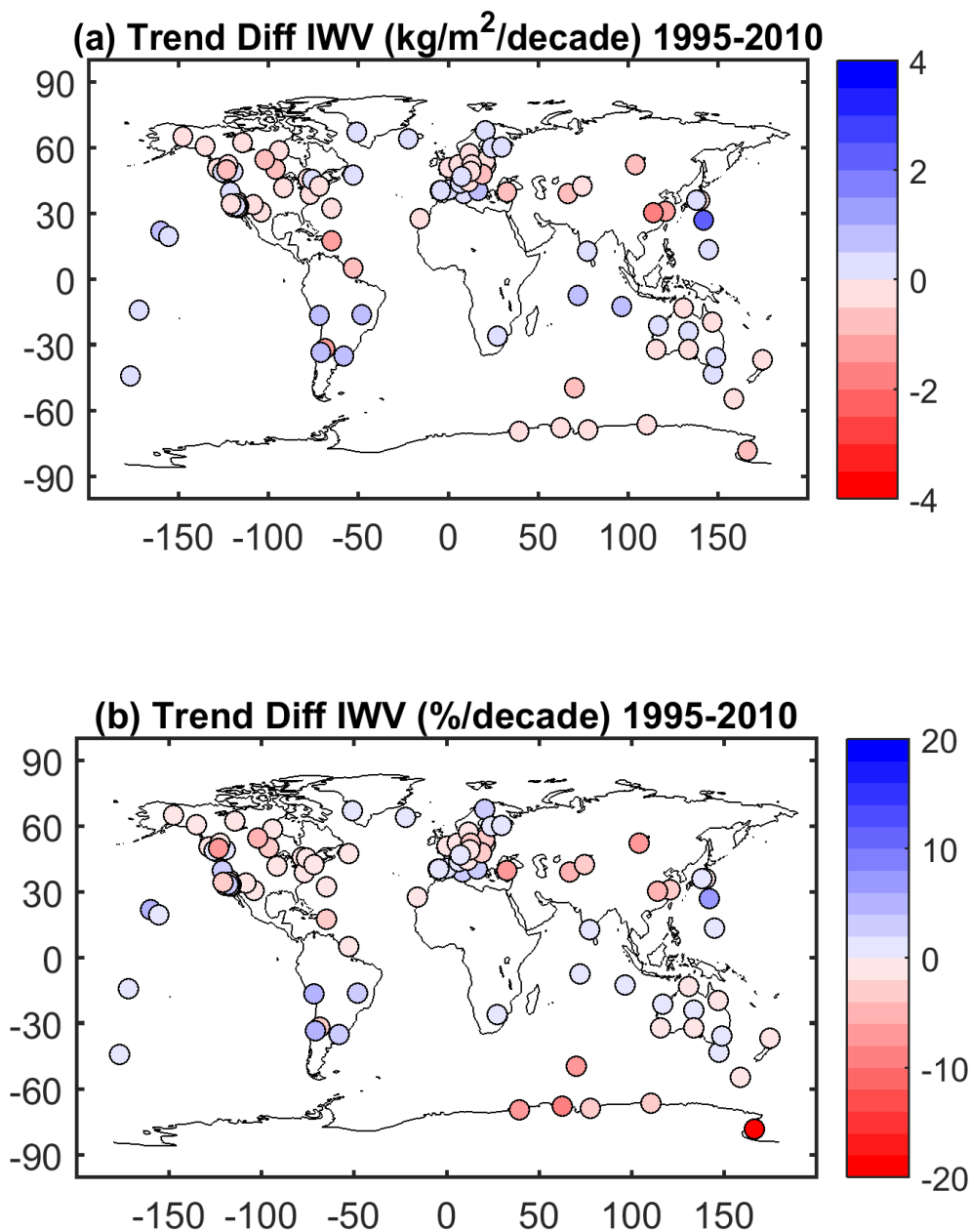


Figure 6: Difference of IWV trends (ERA-Interim minus GPS) for the 1995 to 2010 period, for time-matched series: (a) trends in
5 kg/m^2 per decade and (b) relative trends in $\%$ per decade.

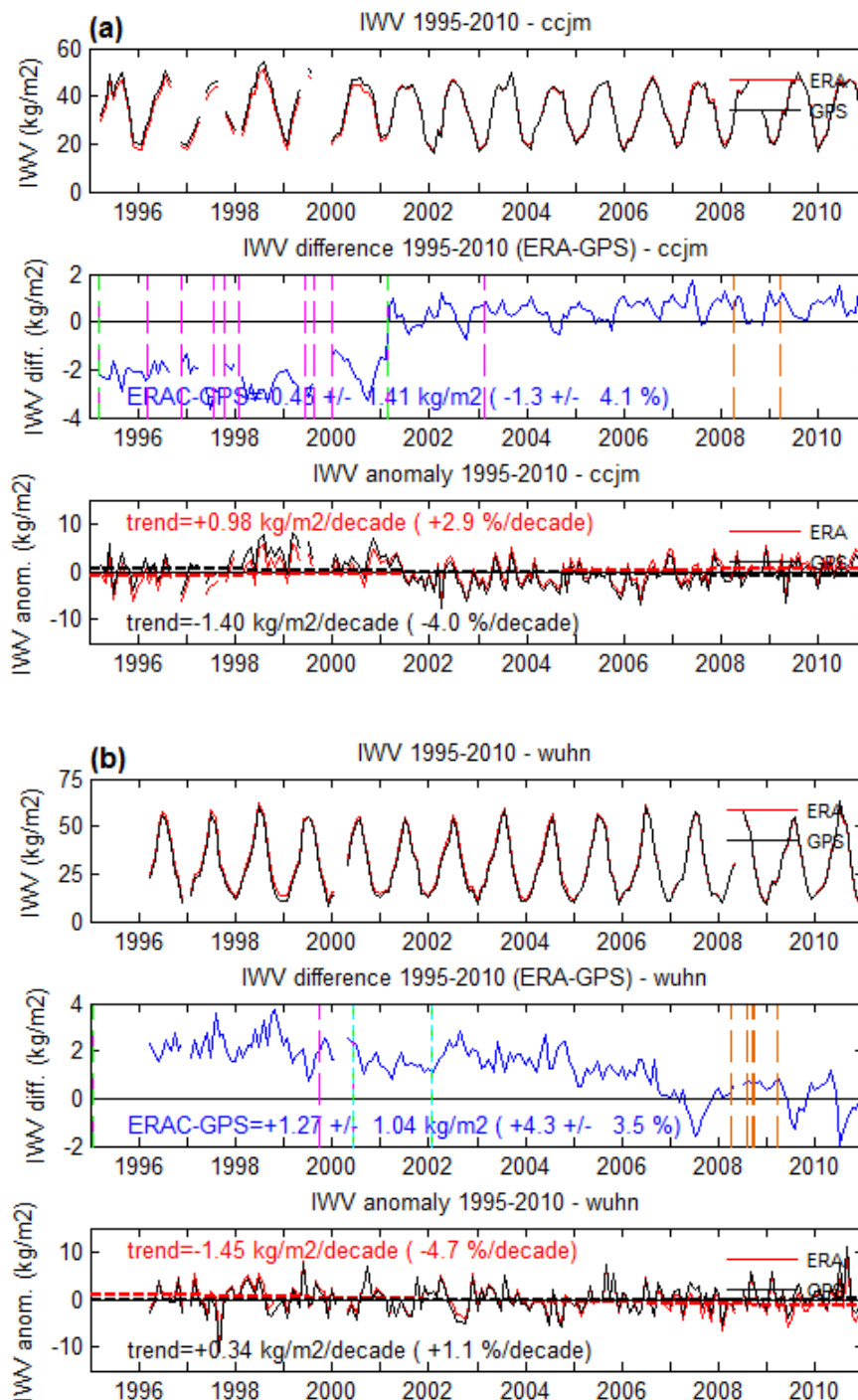


Figure 7: Examples of GPS time series with inhomogeneities: (a) station CCJM and (b) WUHN. Upper plots show IWV for GPS (black) and ERA-Interim (red), middle plots show IWV difference (ERA-Interim minus GPS) and lower plots show monthly anomalies with their linear trend estimates (dashed lines).

5

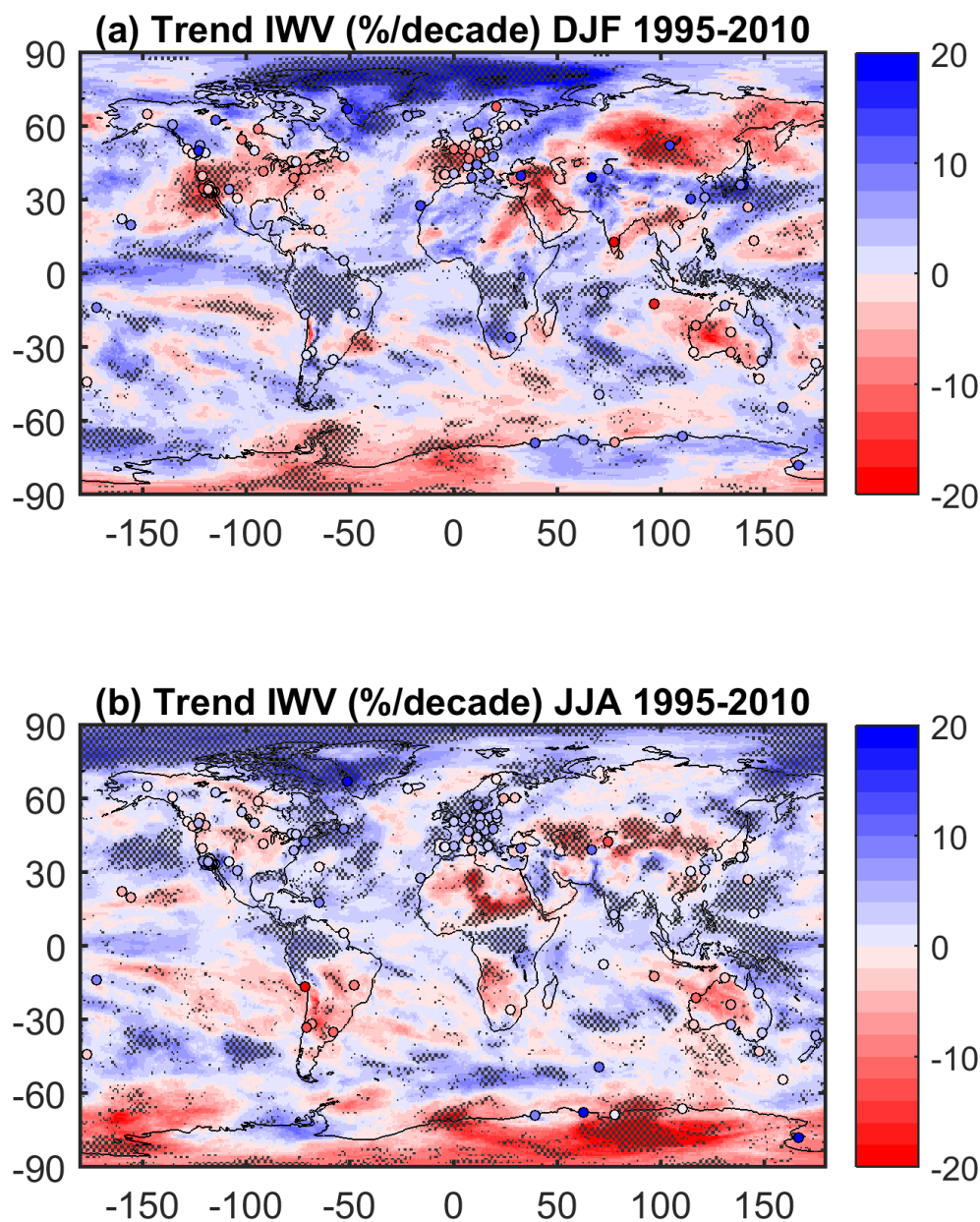


Figure 8: Seasonal IWV trends for the 1995-2010 period from ERA-Interim (shading) and GPS (filled circles) for DJF (a) and JJA (b). The statistically significant trends from ERA-Interim are highlighted by stippling.

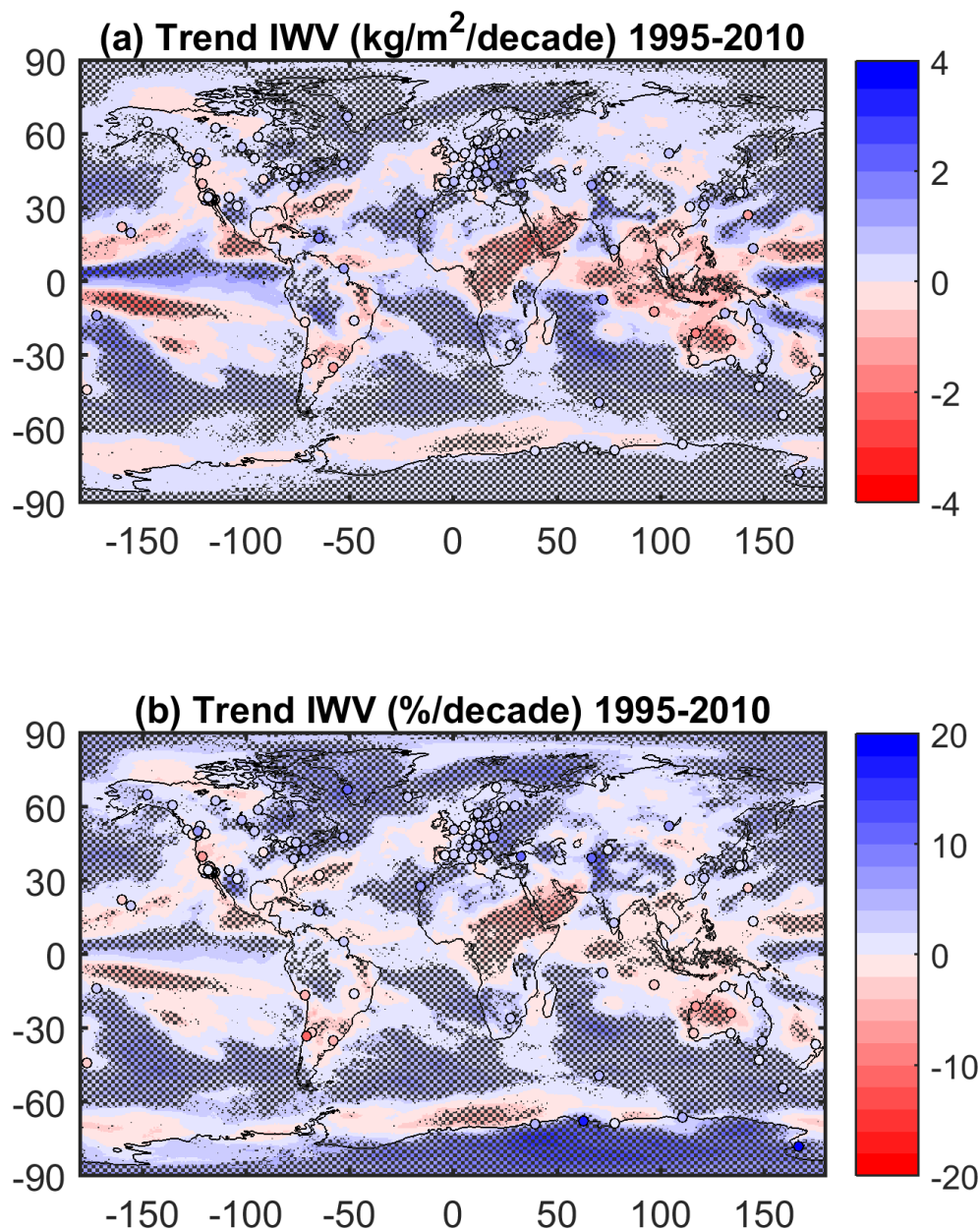
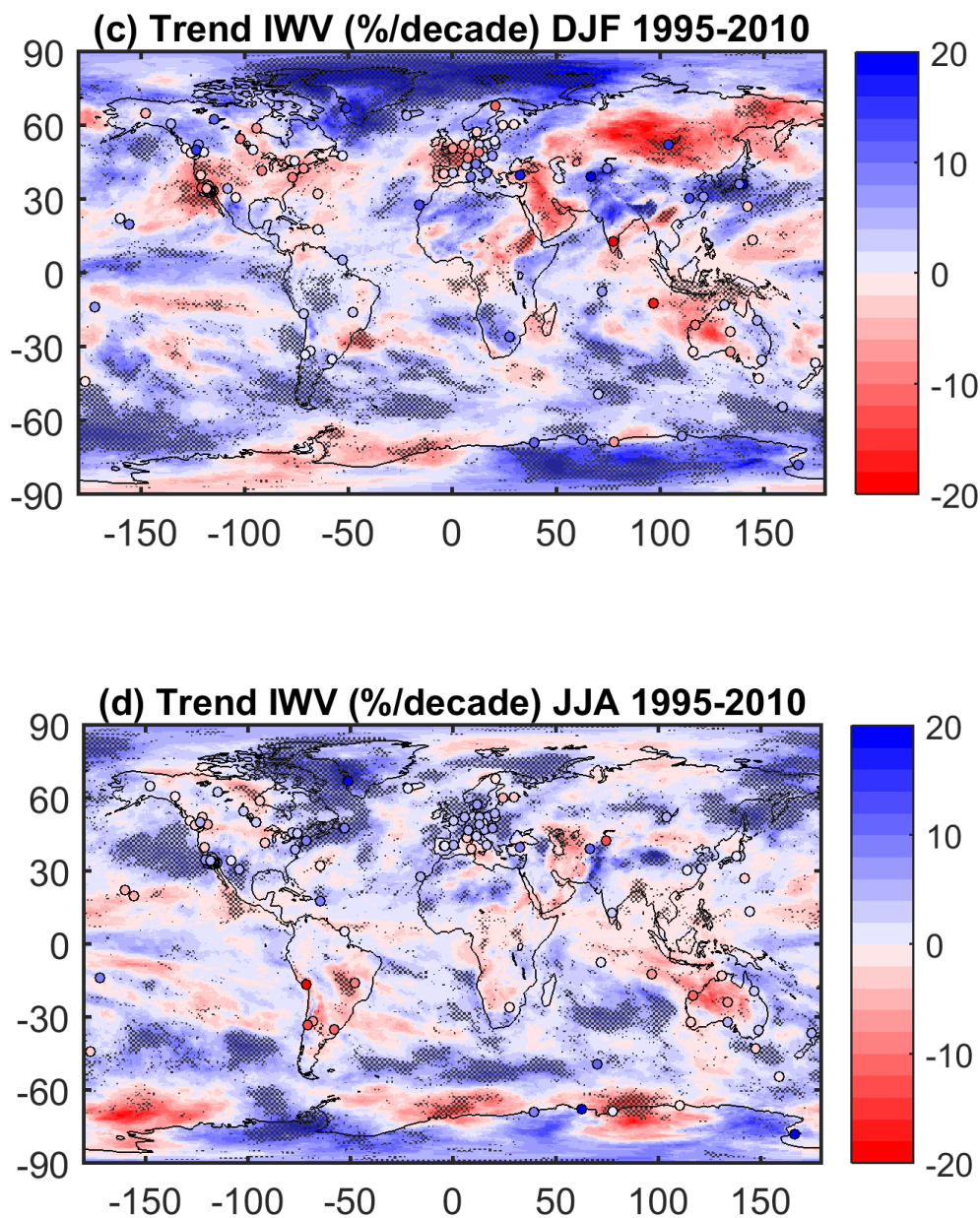


Figure 9: Absolute (a) and relative (b) trends in IWV in the MERRA-2 reanalysis for the 1995-2010 period. The statistically significant trends are highlighted by stippling.



5 **Figure 9 (continued):** Relative trends in IWV in the MERRA-2 reanalysis for the 1995-2010 period for DJF (c) and JJA (d). The statistically significant trends are highlighted by stippling.

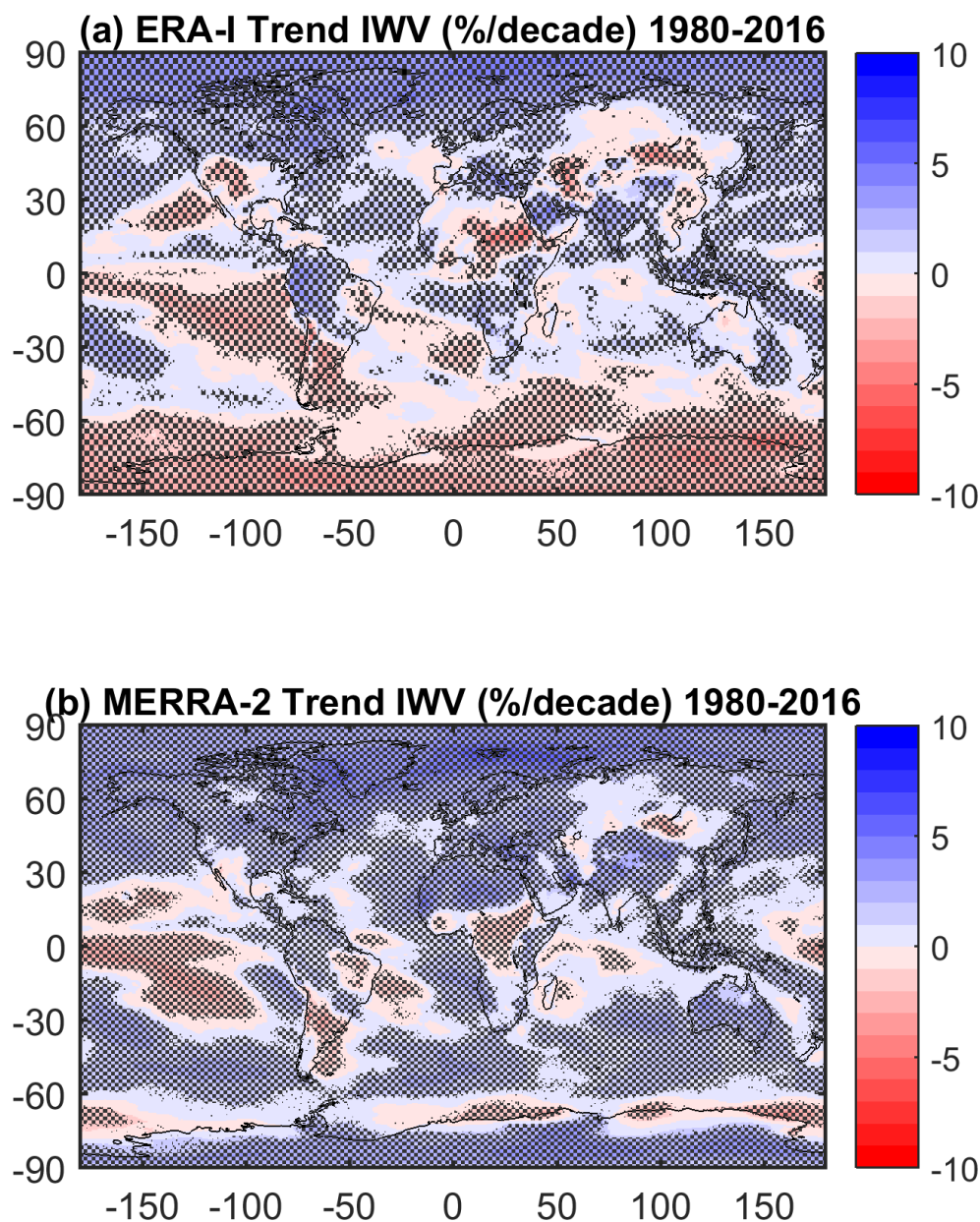


Figure 10: Monthly trends in IWV for the 1980-2016 period for: (a) ERA-Interim, (b) MERRA-2. The statistically significant trends are highlighted by stippling.

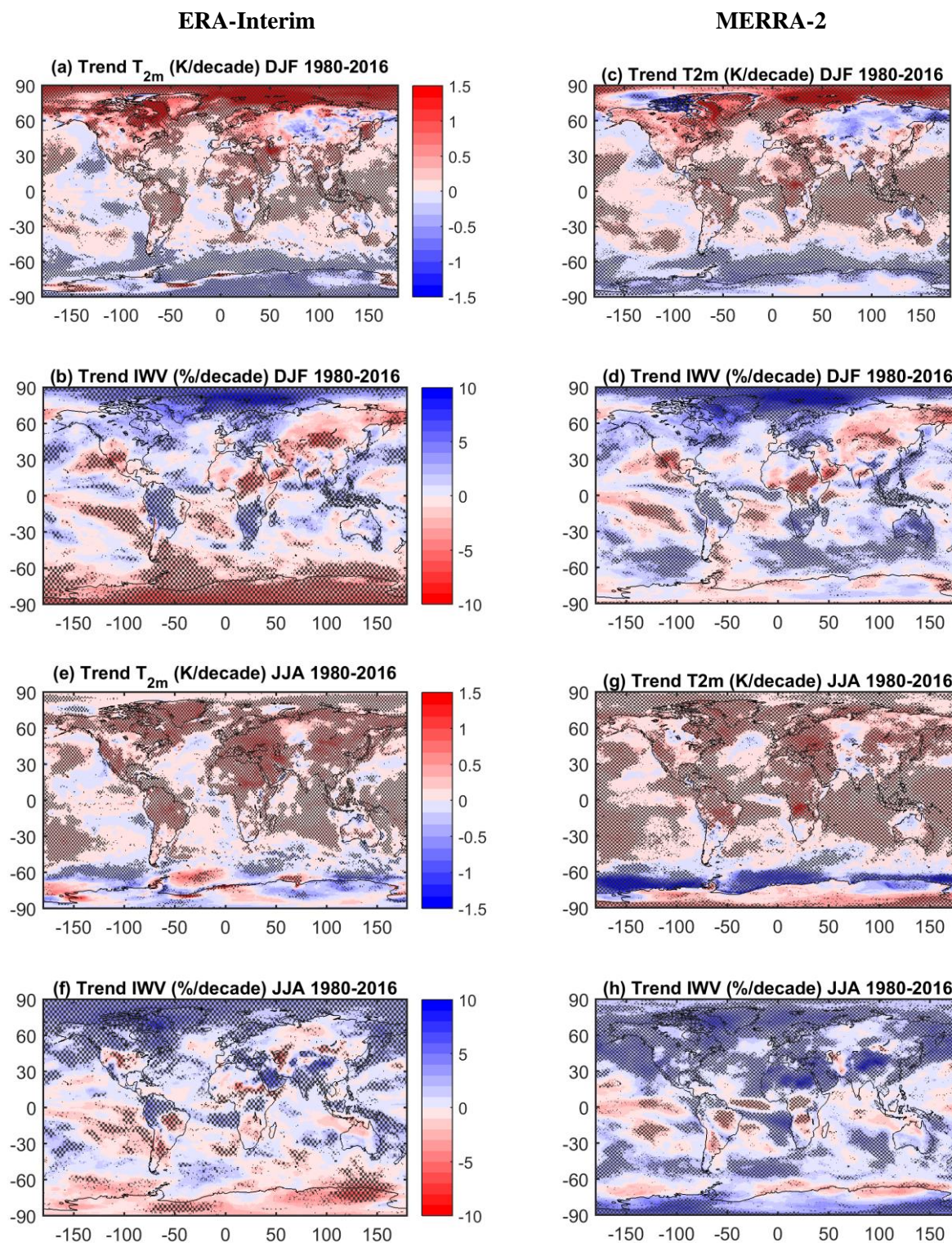


Figure 11: Seasonal trends in T2m and IWV for the 1980 to 2016 period for: (left) ERA-Interim and (right) MERRA-2.

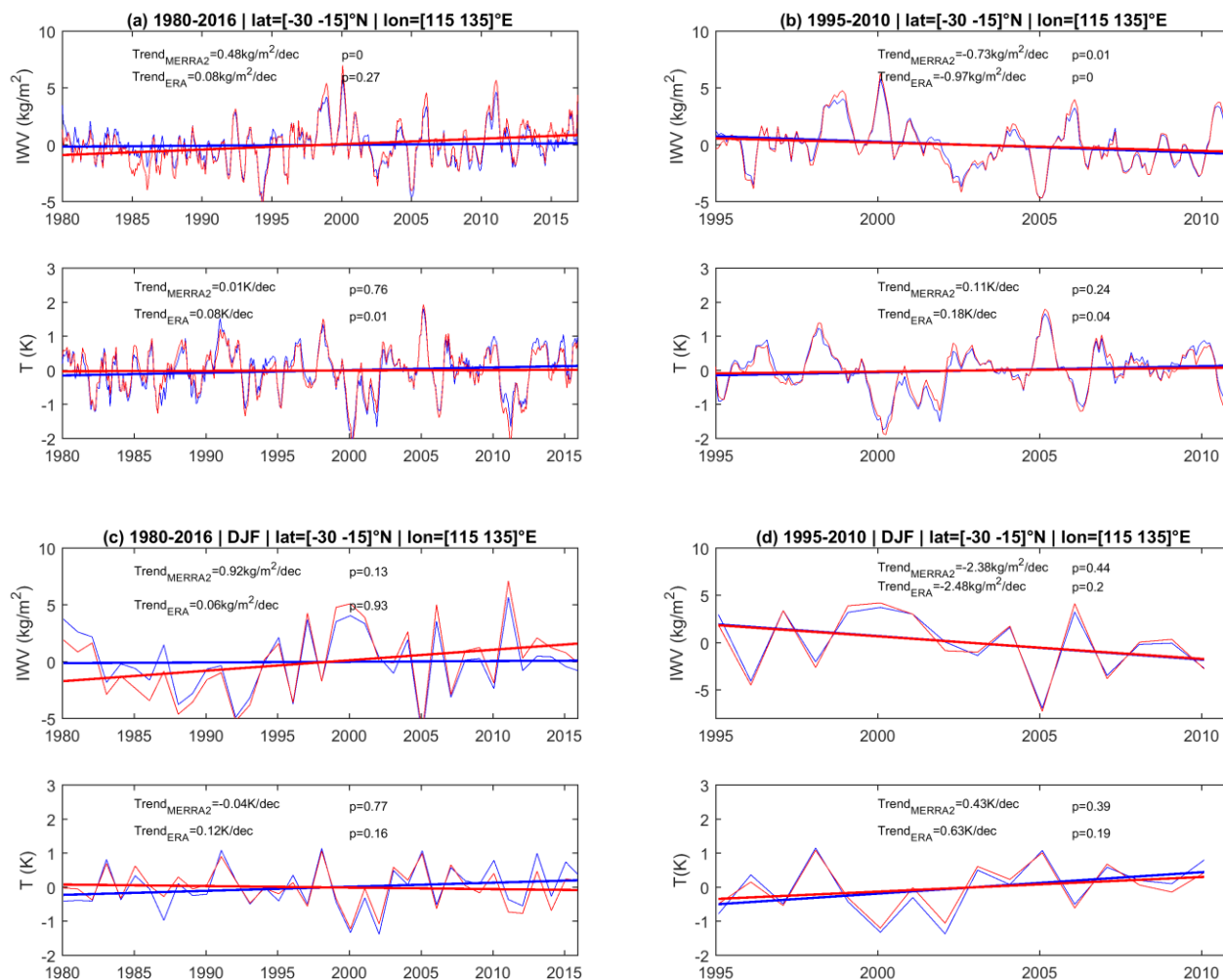


Figure 12: Temperature and IWV anomalies time series for a box over Western Australia (see Fig. 13), using ERA-Interim (blue) and MERRA-2 (red) data, for: (a, c) the 1980 to 2016 period, (b, d) the 1995 to 2010 period, and (a, b) the monthly time series and (c, d) the DJF season.

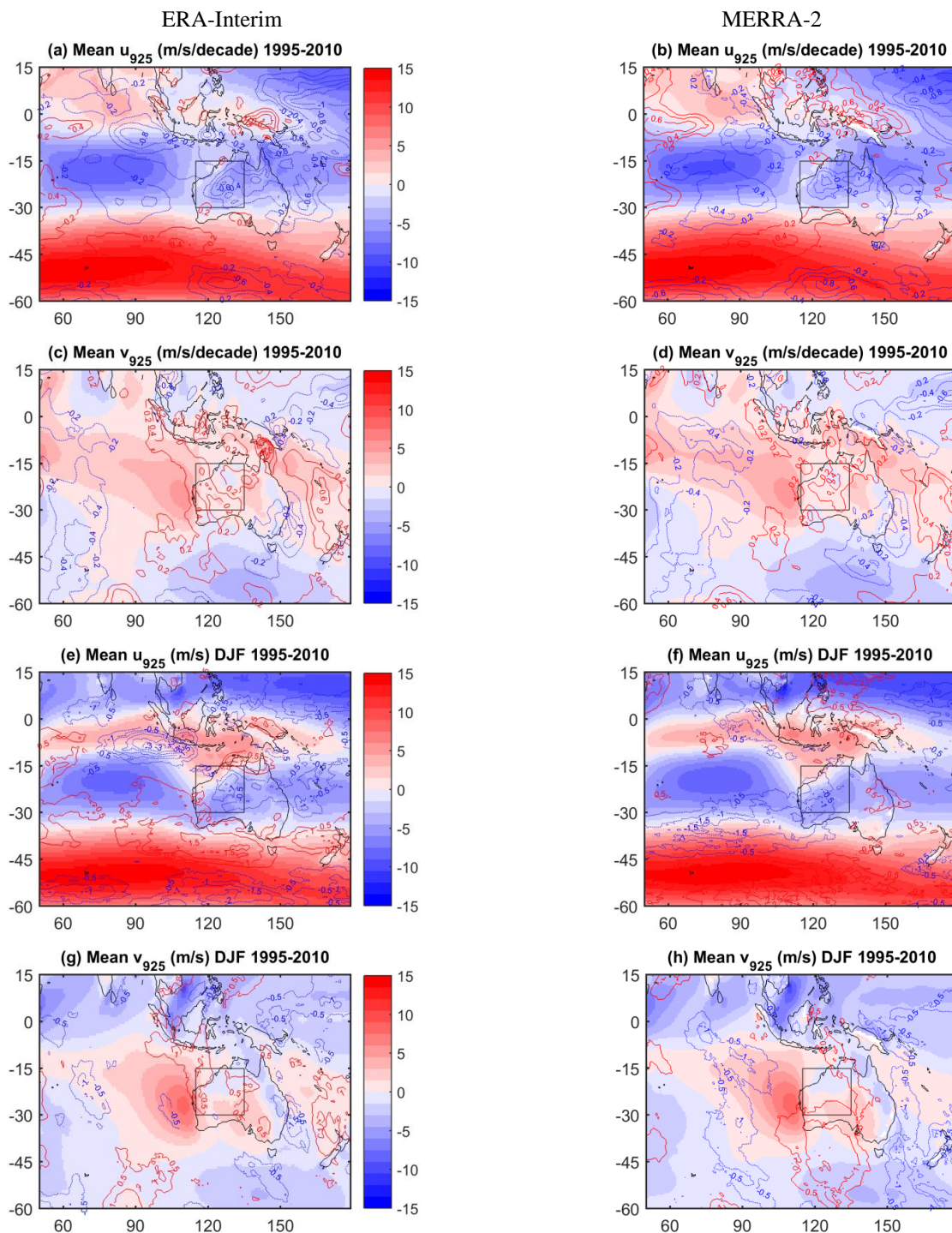


Figure 13: Zoom over Western Australia of the mean monthly and DJF fields and trends of the u and v wind components at 925 hPa (shaded) and their trends (contours). The area of focus (where IWV trends are most intense in ERA-Interim) is marked by a box.

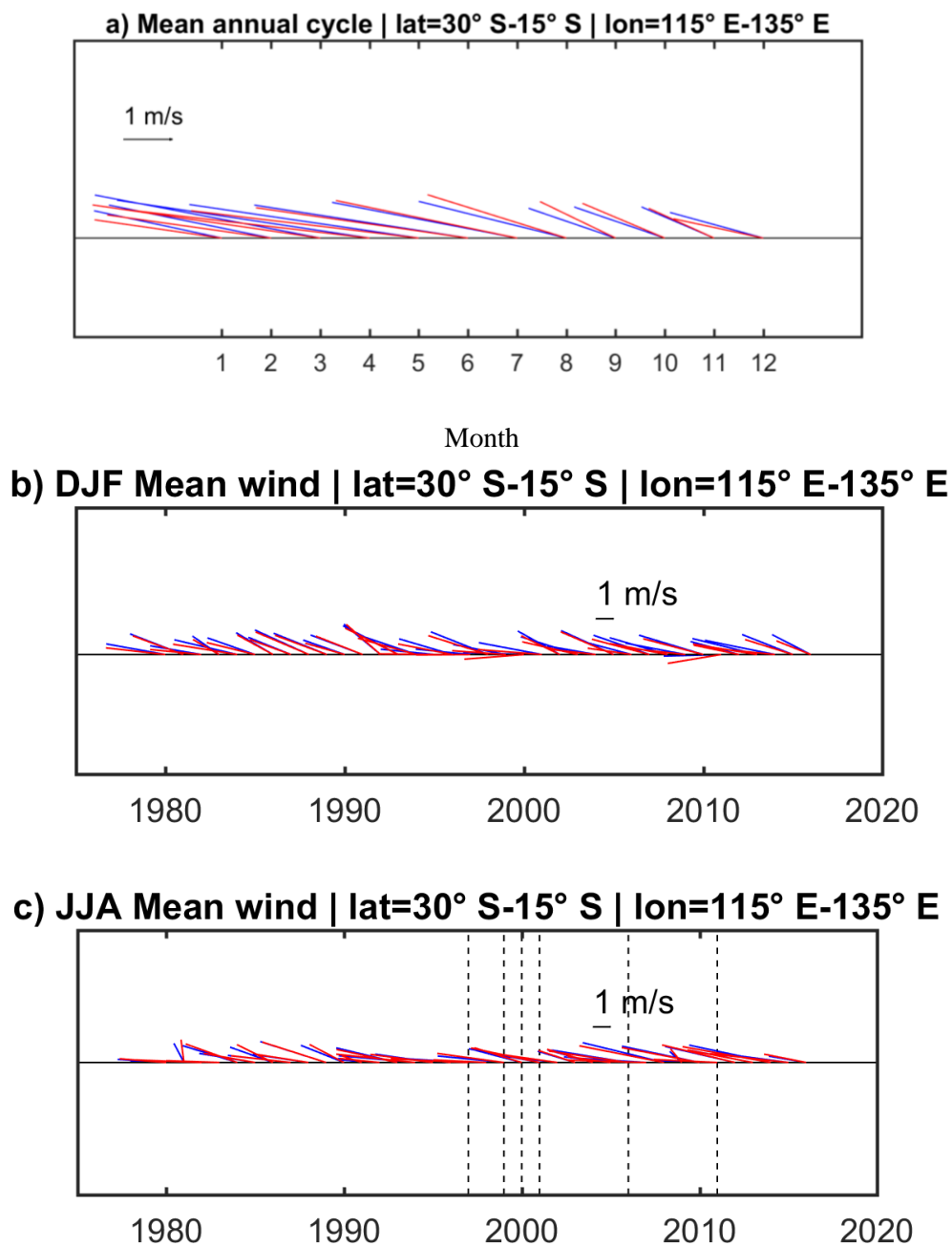


Figure 14: Time series of mean wind vectors for a box over Western Australia (see Fig. 13), using ERA-Interim (blue) and MERRA-2 (red) data, for the 1980–2016 period: mean annual cycle (a), and the monthly time series for the DJF and JJA seasons (b, c).

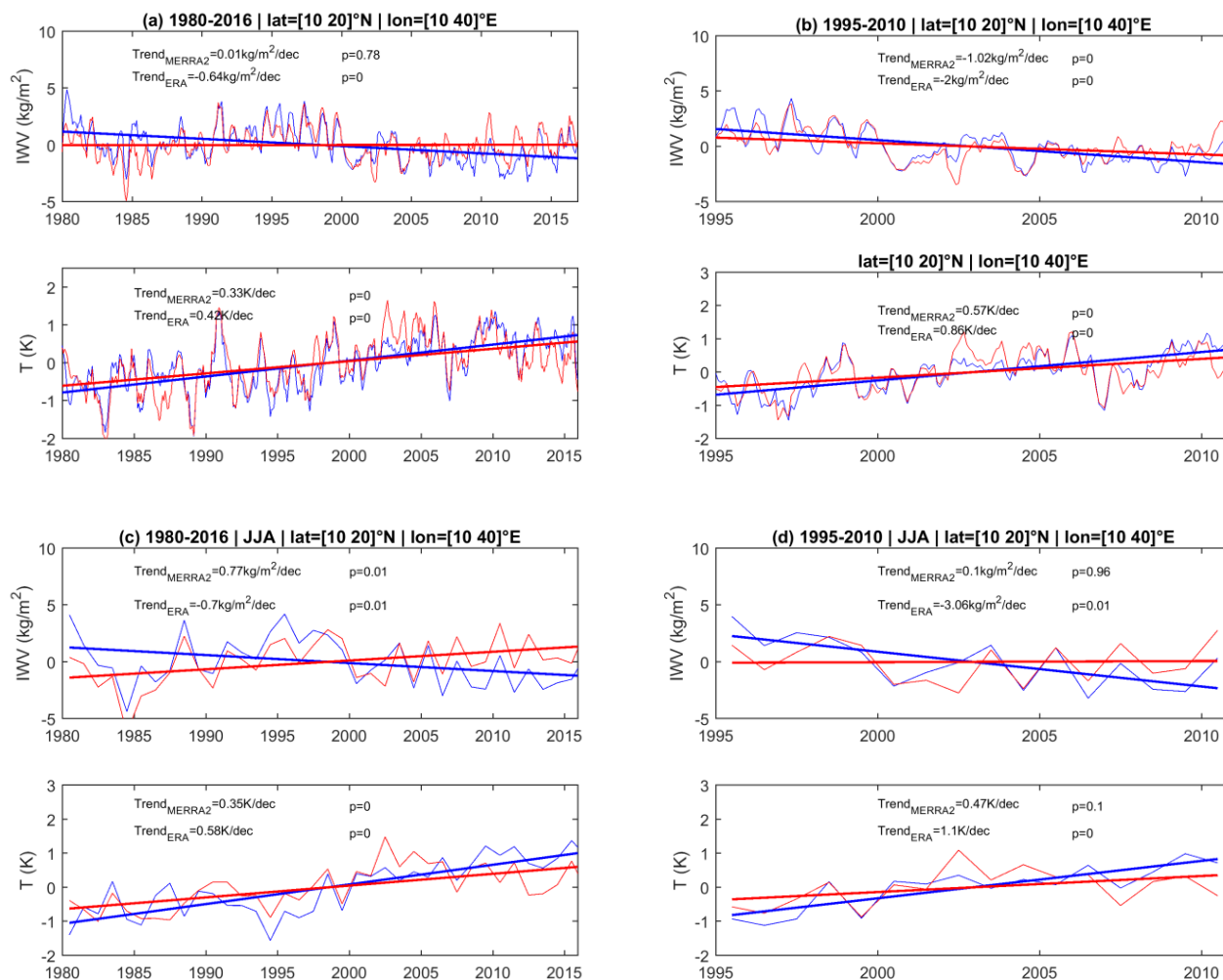


Figure 15: Temperature and IWV anomalies time series for a box over eastern Sahel (see fig. 16), using ERA-Interim (blue) and MERRA-2 (red) data, for: (a, c) the 1980 to 2016 period, (b, d) the 1995 to 2010 period, and (a, b) the monthly time series and (c, d) the JJA season.

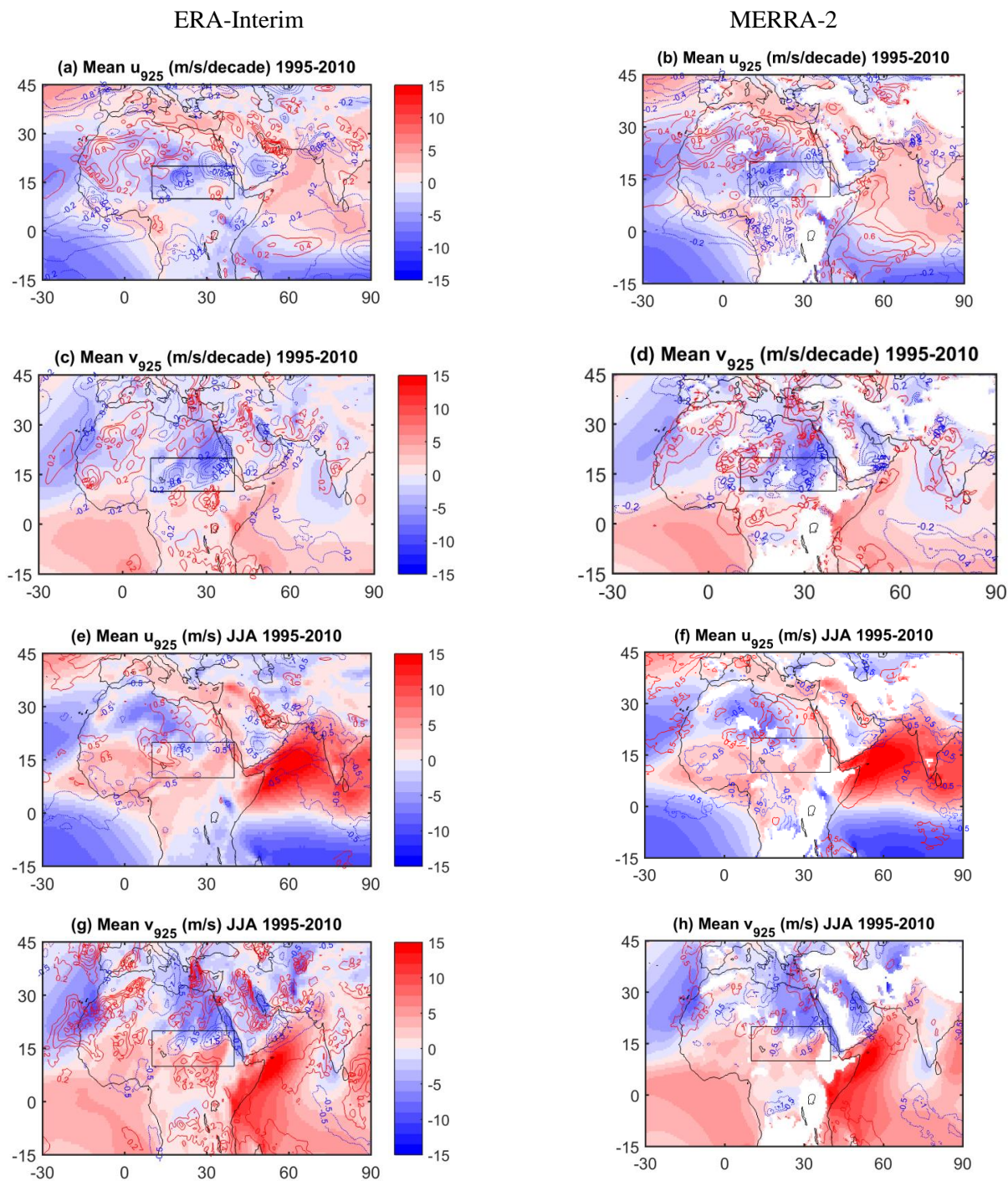


Figure 16: Zoom over North Africa of the mean monthly and JJA fields and trends of the u and v wind components at 925 hPa (shaded) and their trends (contours). The area of focus (where IWV trends are most intense in ERA-Interim) is marked by a box.

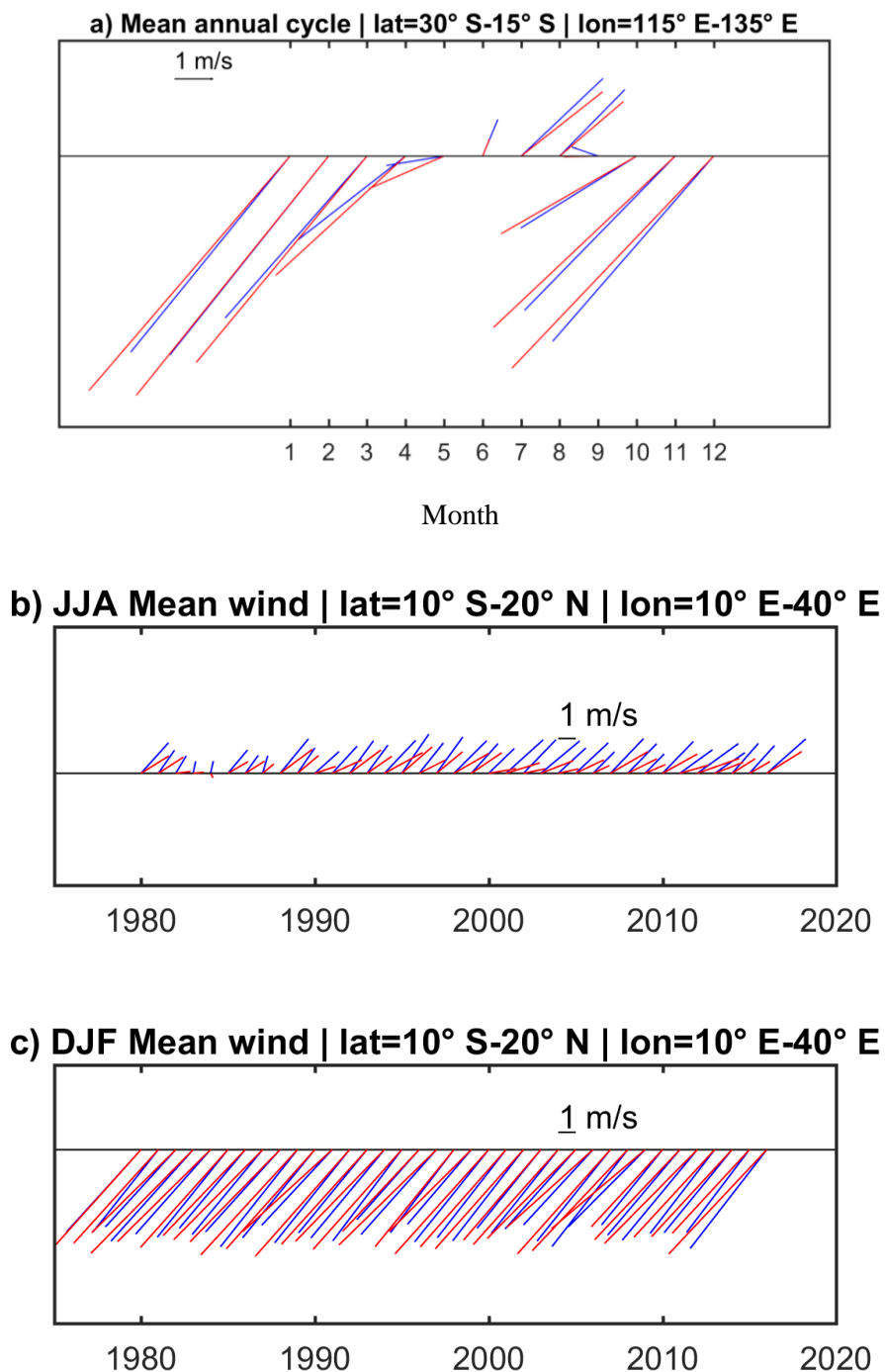


Figure 17: Time series of mean wind vectors for a box over Eastern Sahel (see Fig. 16), using ERA-Interim (blue) and MERRA-2 (red) data, for the 1980–2016 period: mean annual cycle (a), and the monthly time series for the JJA and DJF seasons (b, c).